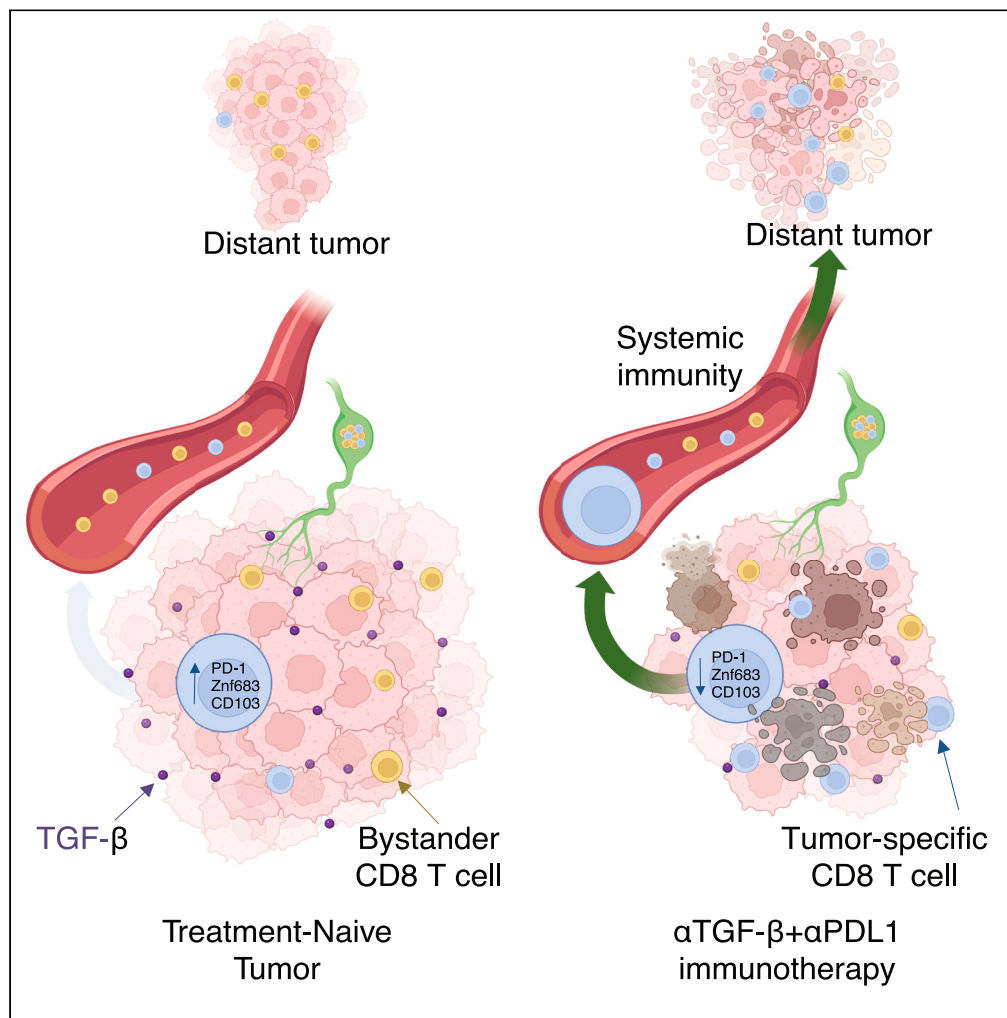


Article

TGF- β neutralization attenuates tumor residency of activated T cells to enhance systemic immunity in mice



Magdalena Fay,
Cem Sievers,
Yvette Robbins, ...,
James L. Gulley,
Clint T. Allen,
Marco Craveiro

clint.allen@nih.gov (C.T.A.)
marco.craveiro@nih.gov (M.C.)

Highlights

TGF- β blockade reduces Znf683 and CD103 in α PDL1-activated TILs

Reduced TIL CD103 expression associates with egress into circulation

The addition of TGF- β blockade to α PDL1 enhances systemic anti-tumor immunity

Circulating CD8⁺ T cells express greater CXCR3 after dual TGF- β and PDL1 blockade



Article

TGF- β neutralization attenuates tumor residency of activated T cells to enhance systemic immunity in mice

Magdalena Fay,¹ Cem Sievers,¹ Yvette Robbins,¹ Xinping Yang,¹ Angel Huynh,¹ Jason M. Redman,² James W. Hodge,² Jeffrey Schlom,² James L. Gulley,² Clint T. Allen,^{1,2,3,*} and Marco Craveiro^{1,*}

SUMMARY

A tissue resident-like phenotype in tumor infiltrating T cells can limit systemic anti-tumor immunity. Enhanced systemic anti-tumor immunity is observed in head and neck cancer patients after neoadjuvant PD-L1 immune checkpoint blockade (ICB) and transforming growth factor β (TGF- β) neutralization. Using T cell receptor (TCR) sequencing and functional immunity assays in a syngeneic model of oral cancer, we dissect the relative contribution of these treatments to enhanced systemic immunity. The addition of TGF- β neutralization to ICB resulted in the egress of expanded and exhausted CD8⁺ tumor infiltrating lymphocytes (TILs) into circulation and greater systemic anti-tumor immunity. This enhanced egress associated with reduced expression of *Itgae* (CD103) and its upstream regulator *Znf683*. Circulating CD8⁺ T cells expressed higher *Cxcr3* after treatment, an observation also made in samples from patients treated with dual TGF- β neutralization and ICB. These findings provide the scientific rationale for the use of PD-L1 ICB and TGF- β neutralization in newly diagnosed patients with carcinomas prior to definitive treatment of locoregional disease.

INTRODUCTION

Tumor-specific T cells harboring a T cell receptor (TCR) specific for tumor antigen encounter many conditions upon entry into the tumor micro-environment (TME) of solid tumors that contribute to their dysfunction. Chronic tumor antigen exposure and the resulting chronic TCR signaling drives expression of immune checkpoints, such as programmed cell death protein-1 (PD-1), that promote T cell exhaustion.^{1–3} Persistent TCR signaling combined with other TME signals such as transforming growth factor β (TGF- β) can also promote a tissue resident-like phenotype that results in the expression of the integrin CD103.^{3,4} Exhausted CD103⁺ tumor infiltrating lymphocytes (TILs) are highly enriched for tumor specificity^{5,6} and represent the population of TILs that respond to PD-based immune checkpoint blockade (ICB) immunotherapy.^{6–10}

Induction of a tissue resident phenotype concentrates retention of tumor-specific T cells in tumors, resulting in low frequencies of T cells with tumor-specificity in circulation.^{6,8} Thus, complete surgical removal of a newly diagnosed primary tumor may also remove most of a patient's reservoir of anti-tumor immunity. Since complete surgical removal of newly diagnosed primary tumors is an accepted primary treatment for many tumor types,¹¹ treatment strategies prior to surgery that aim to rescue tumor-specific TILs from being eliminated by the tumor resection are needed.

Neoadjuvant ICB-based immunotherapy prior to surgical removal of a newly diagnosed primary cancer results in the expansion of tumor-specific TILs within the TME and increased frequency of tumor-specific T cells in circulation.^{6,8} This has been observed in patients with newly diagnosed head and neck squamous cell carcinoma unrelated to human papillomavirus (HNSCC) treated with neoadjuvant ICB.⁸ Combination of ICB and TGF- β neutralization administered to similar patients in the same clinical setting also resulted in the increased frequency of tumor-specific T cells in circulation.⁶ In this work, observed increases in tumor-specific T cells in circulation were tightly associated with a reduction in TGF- β -driven CD103 expression on TILs,^{6,12} indicating that this treatment may reverse tissue resident-like features on T cells in tumors and facilitate their egress into circulation. However, the relative attributions of ICB and TGF- β neutralization to the finding of increased circulating tumor-specific T cells were unclear.

These observations prompted the need for better understanding of whether the addition of TGF- β neutralization results in greater systemic anti-tumor immunity over that observed with ICB alone. Here, using genomic, transcriptomic, and multiple independent functional immune studies, we report greater induction of systemic anti-tumor immunity with combination TGF- β neutralization and programmed death

¹Head and Neck Section, Surgical Oncology Program, Center for Cancer Research, National Cancer Institute, National Institutes of Health, Bethesda, MD, USA

²Center for Immuno-Oncology, Center for Cancer Research, National Cancer Institute, National Institutes of Health, Bethesda, MD, USA

³Lead contact

*Correspondence: clint.allen@nih.gov (C.T.A.), marco.craveiro@nih.gov (M.C.)

<https://doi.org/10.1016/j.isci.2024.110520>



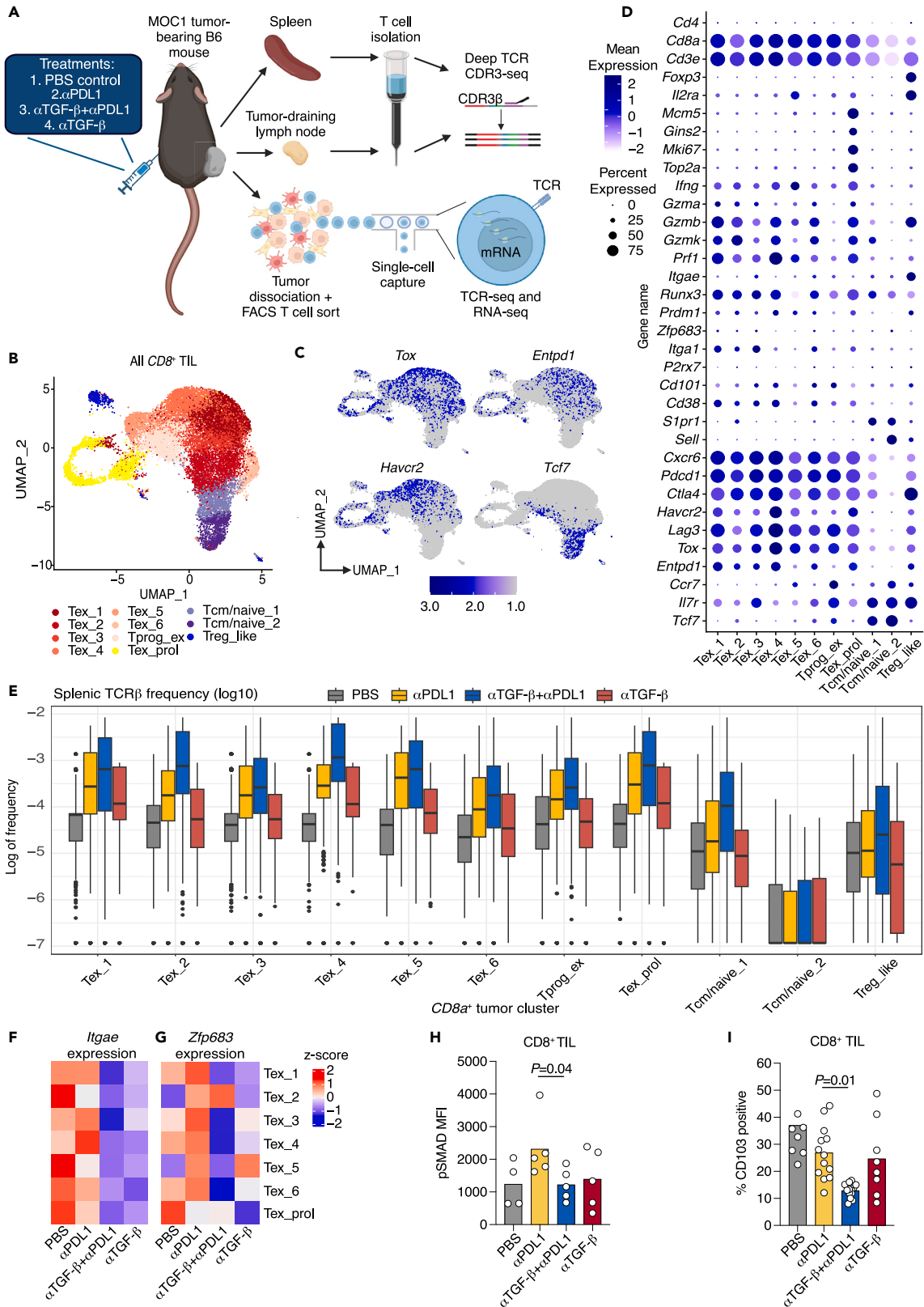


Figure 1. Detection of peripheral TCRs associated with exhausted CD8⁺ TILs was greater with the addition of TGF- β neutralization to PDL1 blockade

- (A) Illustration shows the experimental sequencing approach used to measure changes in the frequency of TCRs associated with TILs in spleens and tumor-draining lymph nodes. FACS, fluorescent-activated cell sorting; CDR, complimentary determining region.
- (B) Scatterplot shows uniform manifold approximation and projection (UMAP) embedding of all CD8⁺ TILs, colored by assigned cluster identify.
- (C) Scatterplot shows UMAP embedding of CD8⁺ TILs, colored by expression of select genes related to activation and exhaustion (*Tox*, *Entpd1*, and *Havcr2*) or stemness (*Tcf7*).
- (D) Dot plot shows expression of select TIL-related genes across CD8⁺ TIL clusters. Circle color corresponds to scaled mean expression; circle size denotes fraction of cells with non-zero gene expression of corresponding gene.
- (E) Box and whisker plots show the frequency of splenic CDR3 TCR β sequences matched to CD8⁺ TIL TCRs for individual TIL clusters and colored by treatment condition. Significance between treatment conditions for each cluster, determined by a Wilcoxon test, is listed in the supplemental data file. $n = 5$ mice per treatment group.
- (F and G) Heatmaps show the relative expression of (F) *Itgae* or (G) *Znf683* in exhausted CD8⁺ TILs. Significance between the exhausted CD8⁺ TILs from the α TGF- β + α PDL1 and α PDL1 treatment conditions, determined with a Wilcoxon test, is listed in the supplemental data file. $n = 5$ mice per treatment group.
- (H) Bar plot shows the median fluorescence intensity (MFI) of pSMAD2^{S465/S467}/3^{S423/S425} expression in CD8⁺ TILs measured by flow cytometry. $n = 4-5$ mice per treatment group. Significance between treatment groups was determined with a Mann-Whitney test.
- (I) Bar plot show percentage of CD8⁺ TILs positive for CD103 as measured by flow cytometry. $n = 7-13$ mice per treatment group. Significance between treatment groups was determined with a Mann-Whitney test.

ligand 1 (PDL1) ICB compared to PDL1 ICB alone in a syngeneic model of carcinoma. Mechanistically, the addition of TGF- β neutralization to PDL1 ICB resulted in reduced expression of the tissue residency markers *Znf683* (Hobit) and *Itgae* (CD103) in exhausted and expanded TILs as well as increased expression of *Cxcr3* on circulating T cells, a finding also observed in archived peripheral blood mononuclear cells (PBMC) clinical samples from patients treated with dual TGF- β neutralization and PDL1 ICB in a prospective clinical study.¹³ These observations link TGF- β signaling in ICB-activated T cells to multiple processes regulating tissue residency and T cell trafficking in cancer and validate the addition of TGF- β neutralization to ICB as an effective strategy to maximize systemic anti-tumor immunity.

RESULTS

Addition of TGF- β neutralization to anti-PDL1 increases frequencies of clonotypes associated with exhausted TILs in circulation

Genomic approaches have been used to demonstrate increased tumor-specific T cells in circulation after neoadjuvant immunotherapy in human clinical specimens.^{6,8} To study the dynamics of T cell compartmentalization with a similar approach following PDL1 blockade alone or in combination with TGF- β neutralization, we generated syngeneic, carcinogen-induced murine oral cancer 1 (MOC1) tumors with genomic, transcriptomic and immunologic similarity to human HNSCC in wild-type C57BL/6 (WT B6) mice.¹⁴ Mice bearing established MOC1 tumors (volume ≥ 0.1 cm³) were treated with three doses of the anti-PDL1 mAb avelumab (hereafter referred to as α PDL1), dual TGF- β neutralization and anti-PDL1 mAb bintrafusp alfa (formerly known as M7824, hereafter referred to as α TGF- β + α PDL1),¹⁵ bintrafusp alfa with a mutated non-functional PDL1 binding domain (hereafter referred to as α TGF- β), or PBS control. The α PDL1 and α TGF- β + α PDL1 compounds were doses to >90% PD-L1 target occupancy.¹⁵ Two days after completing treatment, TCR sequences and gene expression profiles of TILs were determined by single-cell RNA and TCR sequencing. Splenic and tumor draining lymph node (tdLN) TCR sequences were determined by deep TCR sequencing. This allowed matching of tumor, spleen (reflective of peripheral circulation), and tdLN TCR sequences in individual mice as a measure of T cell compartmentalization and study of how this changed with treatment (Figures 1A and S1A, 5 mice per group). After determining individual CD8a⁺ and CD4⁺ TIL clonotypes (Figure S1B), clustering of CD8a⁺ TILs revealed numerous exhausted clusters harboring gene expression profiles associated with TCR-engagement and tumor antigen-specificity in human cancers.^{6,16,17} Specifically, multiple clusters displayed markers of exhaustion (*Tox*, *Pdcd1*, *Ctla4*, *Havcr2*, and *Lag3*), activation (*Ifng*, *Gzmb*, *Prf1*, *Cxcr6*, and *Entpd1*), and tissue residency (*Itga1*, *Runx3*, and *Prdm1*), referred to as Tex clusters 1–6 (Figures 1B–1D and S1C), with the four largest clusters being Tex_1–4 (Figure S1D). Exhausted proliferating (Tex_prol, *Mki67*, and *Top2a*), exhausted progenitor (Tprog_ex, *Ccr7*, *Il7r*, and *Tcf7*) and naive or central memory clusters were also observed. Clustering of CD4⁺ TILs revealed several *Foxp3*⁺*Il2ra*⁺*Ctla4*⁺ Treg clusters (Treg_1–3), an exhausted cluster (Tex) and stem-like and naive or central memory clusters (Figures S1E–S1H).

Notably, splenic and tdLN TCR sequences originating from the same mouse had a greater Jaccard similarity coefficient compared to TCR sequences originating from different mice (Figure S2A). We next matched splenic and tdLN TCR sequences with TCR sequences associated with each CD8a⁺ and CD4⁺ TILs cluster from individual mice and measured differences in shared TCR β sequences by treatment. This revealed a significant increase in splenic TCR β frequencies across all exhausted and the Tcm/naive CD8a⁺ clusters in mice treated with α PDL1 or α TGF- β + α PDL1 compared to control or α TGF- β alone, with a significantly greater increase in α TGF- β + α PDL1 treated mice compared to α PDL1 treated mice (Figure 1E, supplemental data file, $p = 0.03$ to $p = 4.3 \times 10^{-52}$). Similar findings were not observed or were observed less consistently when considering matched tdLN and CD8a⁺ TILs TCR β sequences (Figure S2B) or when considering spleen or tdLN TCR β sequences matched with CD4⁺ TIL TCR sequences (Figures S2C and S2D). These data indicated that α TGF- β + α PDL1 treatment, and to a lesser degree α PDL1 treatment, resulted in the selective increase of CD8a⁺ T cells in circulation (spleen) that share TCR β sequences with exhausted T cells in the tumor. The finding that α TGF- β + α PDL1 treatment in mice drives egress of CD8a⁺ TILs into circulation is consistent with observations of increased circulation of exhausted TILs made in HNSCC patients following treatment with bintrafusp alfa.⁶ Given prior associations between an exhausted TIL phenotype and tumor-specificity, increased detection of exhausted T cells in circulation following treatment likely

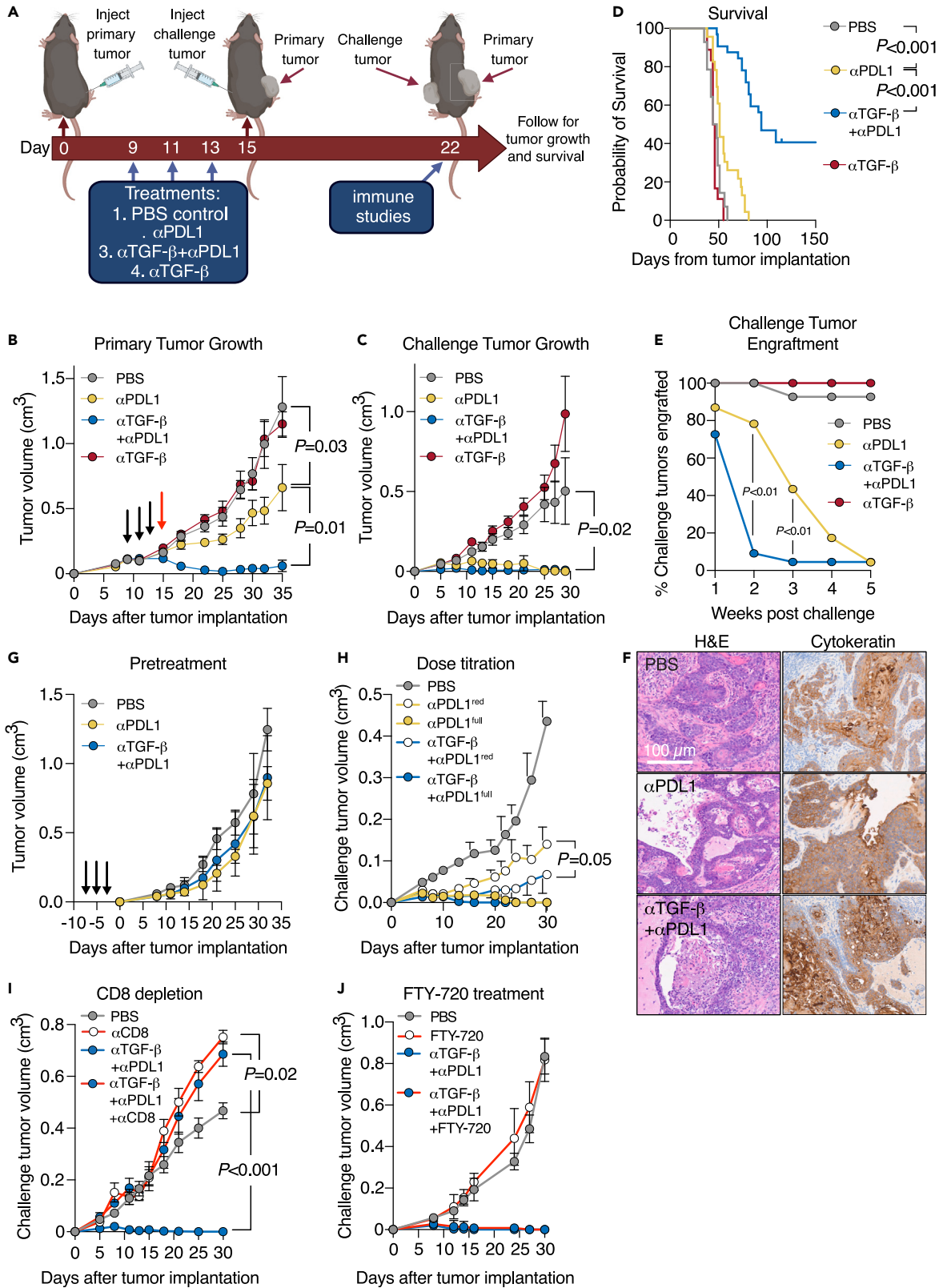


Figure 2. Kinetics of challenge tumor rejection observed with PDL1 blockade were enhanced with the addition of TGF- β neutralization

- (A) Illustration shows the experimental approach to functional assessment of systemic anti-tumor immunity using engraftment of a secondary challenge tumor.
- (B) Line graph shows primary tumor growth curves, colored by treatment. $n = 15$ – 20 mice per treatment group. Significance was determined with one-way ANOVA with multiple comparisons, considering tumor volume from the start of treatment (day 9). Black arrows correspond to treatments. The red arrow corresponds to challenge tumor engraftment (2 days after completion of treatment).
- (C) Line graph shows challenge tumor growth curves, colored by treatment. $n = 15$ – 20 mice per treatment group. Significance was determined with one-way ANOVA with multiple comparisons, considering tumor volume from engraftment (day 0).
- (D) Kaplan-Meier plot shows survival, colored by treatment. $n = 15$ – 20 mice per treatment group. Significance was determined with a log rank test.
- (E) Line graph shows the percentage of mice with engrafted tumors, colored by treatment. Significance between α PDL1 and α TGF- β + α PDL1 engraftment rates was determined at each time point with a Fisher's exact test.
- (F) Representative photomicrographs of tumor sections stained with hematoxylin and eosin (H&E, left) or a pan-cytokeratin antibody (right), by treatment condition.
- (G) Line graph shows tumor growth curves following treatment of mice prior to tumor engraftment. Black arrows indicate pre-treatments. $n = 5$ mice per treatment group.
- (H) Line graph shows challenge tumor growth curves, colored by treatment with either full dose α PDL1 (350 μ g/injection) or α PDL1 and α TGF- β + α PDL1 (492 μ g/injection) or reduced dose α PDL1 (35 μ g/injection) or α PDL1 and α TGF- β + α PDL1 (49.2 μ g/injection). Significance was determined with one-way ANOVA with multiple comparisons, considering tumor volume from engraftment (day 0). $n = 5$ – 10 mice per treatment group.
- (I) Line graph shows challenge tumor growth curves, colored by treatment with α TGF- β + α PDL1 alone or in combination with CD8 depletion. Significance was determined with one-way ANOVA with multiple comparisons, considering tumor volume from engraftment (day 0). $n = 10$ mice per treatment group.
- (J) Line graph shows challenge tumor growth curves, colored by treatment with α TGF- β + α PDL1 alone or in combination with FTY-720 administered beginning two days before treatment (day 7), 30 μ g IP/injection, and continued every other day for three weeks. $n = 10$ mice per treatment group.

represented direct genomic measurement of enhanced systemic anti-tumor immunity following treatment with α PDL1 and more specifically α TGF- β + α PDL1. Mechanistically, movement from the tumor into circulation suggested that tissue residency needed to be reversed in one or more subsets of exhausted CD8⁺ TILs.

CD103 (*Itgae*) is a TGF- β -induced T cell adhesion molecule associated with tissue residency, and a reduction in CD8a⁺ T cell *Itgae* expression was observed in HNSCC patients treated with bintrafusp alfa.⁶ Analysis of CD8a⁺ TILs in this murine dataset revealed reduced expression of *Itgae* and the tissue residency-associated transcription factor *Znf683* following treatment with α TGF- β + α PDL1 or α TGF- β compared to α PDL1 or control (Figures 1F and 1G). In turn, α PDL1 treatment rendered CD8⁺ TILs responsive to TGF- β signaling with increased SMAD2/3 phosphorylation (Figure 1H), while a significant reduction in phosphorylation of SMAD2/3 was observed in CD8⁺ TILs from α TGF- β + α PDL1 treated mice, confirming a reduction in signaling downstream of the TGF- β receptor following TGF- β neutralization. Validating the reduction in *Itgae* transcripts at the protein level, reduced cell surface CD103 expression measured by flow cytometry was also observed on CD8⁺ TILs from mice treated with α TGF- β + α PDL1 compared to mice treated with α PDL1 (Figure 1I). Additionally, increased CD103 expression on CD8⁺ murine T cells stimulated *in vitro* with CD3/28 and TGF- β , but not CD3/28 alone, was reduced to baseline in the presence of α TGF- β + α PDL1 or α TGF- β (Figure S3A). These results suggested that increased frequencies of exhausted CD8a⁺ TIL-associated TCR frequencies in the circulation of mice were noted following α PDL1 or α TGF- β + α PDL1 treatment, which indicates that T cell reactivation following α PDL1 ICB is a necessary step in egress. Furthermore, the data show that a reduction in TGF- β -induced CD103 expression on CD8⁺ T cells underlies the increased frequency in circulating CD8a⁺ TILs observed following α TGF- β + α PDL1 compared to α PDL1.

The addition of TGF- β neutralization to PDL1 blockade enhanced functional systemic anti-tumor immunity beyond that observed with PDL1 alone

To test whether the observed increases in exhausted CD8⁺ TIL-associated splenic TCR frequencies after α PDL1 or α TGF- β + α PDL1 treatment are associated with functional increases in systemic anti-tumor immunity, we performed tumor challenge experiments where the ability of the immune system to control the engraftment or growth of a contralateral challenge tumor implanted after treatment was studied (Figure 2A). Mice bearing established MOC1 tumors (volume ≥ 0.1 cm³) were treated, and a contralateral tumor challenge was implanted two days after treatment completion to use as a readout of change in systemic anti-tumor immunity. Although both α PDL1 and α TGF- β + α PDL1 delayed primary tumor growth compared to α TGF- β or control, α TGF- β + α PDL1 treatment resulted in greater primary tumor growth control compared to α PDL1 (Figure 2B). Considering secondary challenge tumors as a readout of systemic immunity, both α PDL1 and α TGF- β + α PDL1 treatments resulted in the control and eventual rejection of challenge tumors in all mice (Figure 2C). This result implied enhanced systemic anti-tumor immunity following both α PDL1 and α TGF- β + α PDL1 treatments compared to α TGF- β or control. α TGF- β + α PDL1 treatment resulted in prolonged survival compared to α PDL1 treatment (Figure 2D), but this was primarily driven by greater primary tumor growth control with α TGF- β + α PDL1. Close study of the kinetics of secondary challenge tumor rejection, by considering the proportion of challenge tumors that remained engrafted over time, revealed that α TGF- β + α PDL1 treatment resulted in rejection of a greater proportion of challenge tumors at the 2- and 3-week time points after challenge compared to α PDL1 treatment (Figure 2E). Carcinomas were detected upon histologic analysis of challenge tumors harvested 1 week after challenge engraftment (Figure 2F), confirming that challenge tumors do indeed engraft and are subsequently rejected in mice treated with α PDL1 or α TGF- β + α PDL1. Thus, both α PDL1 and α TGF- β + α PDL1 treatments result in systemic immunity of sufficient magnitude to eventually reject challenge tumors, but study of the kinetics of challenge tumor rejection suggests that the magnitude of the systemic immune response after α TGF- β + α PDL1 may be greater compared to α PDL1 since challenge tumors in α TGF- β + α PDL1 treated mice reject faster.

To rule out the possibility that α PDL1 or α TGF- β + α PDL1 treatment non-specifically enhanced systemic T cells that resulted in rejection of challenge tumors, naive mice were treated prior to primary tumor injection. Primary MOC1 tumor growth in mice treated with α PDL1 or α TGF- β + α PDL1 prior to engraftment was similar to mice treated with PBS prior to engraftment (Figure 2G), indicating that these treatments do not result in non-specific systemic activation of T cells that can prevent challenge tumor engraftment. These results also indicate that a primary tumor must be present at the time of treatment to observe the enhanced systemic anti-tumor immunity after α PDL1 or α TGF- β + α PDL1 treatment, supporting the hypothesis that the tumor-specific T cells conferring enhanced systemic anti-tumor immunity need to be primed and likely undergo expansion within the primary tumor or tLN for the treatment to work.

We next studied whether a dose effect on the induction of systemic anti-tumor immunity could be observed by treating mice bearing established MOC1 tumors with a reduced dose of α PDL1 or α TGF- β + α PDL1 (1/10th of the full dose) prior to challenge. Greater control of challenge tumor growth was observed with reduced-dose α TGF- β + α PDL1 compared to reduced dose α PDL1 (Figure 2H), suggesting measurably greater systemic anti-tumor immunity with α TGF- β + α PDL1 at lower doses compared to lower doses of α PDL1. To dissect the effector cell types responsible for challenge tumor control after α TGF- β + α PDL1 treatment, T cell depletion studies were performed. CD8 depletion totally abrogated (Figure 2I) and CD4 depletion partially abrogated (Figure S3B) challenge tumor growth control, indicating that elimination of the challenge tumor is primarily CD8⁺ T cell dependent with some contribution or help from CD4⁺ T cells. Additionally, growth control of challenge tumors was observed following CD4 depletion alone when compared to PBS treatment alone, which can possibly be explained by the depletion of regulatory T cells (Tregs) known to induce immunosuppression in the TME. Finally, challenge tumor growth following α TGF- β + α PDL1 treatment was studied in the presence of FTY-720 treatment that inhibits egress of T cells from secondary lymphoid tissues (such as tLN). FTY-720 treatment did not alter the ability of α TGF- β + α PDL1 treatment to result in complete challenge tumor rejection (Figure 2J), suggesting that the enhanced systemic anti-tumor immunity observed after α TGF- β + α PDL1 treatment does not involve egress of tumor-specific T cells from the tLN. Together, these data indicated that although both α PDL1 and α TGF- β + α PDL1 treatment resulted in enhanced systemic anti-tumor immunity, α TGF- β + α PDL1 treatment results in CD8-dependent systemic anti-tumor immunity of greater magnitude than that observed with α PDL1 treatment. Further, the paired TCR-seq and FTY-720 treatment data suggest that tumor-specific T cells originating from the primary tumor are sufficient to control the challenge tumor.

We next studied differences in the immune microenvironment of challenge tumors by treatment condition. Flow cytometric analysis of challenge tumors revealed greater CD8⁺ TIL infiltration in mice treated with α PDL1 or α TGF- β + α PDL1, although greater frequency of CD8⁺ TILs following α TGF- β + α PDL1 was observed when compared to α PDL1 (Figure 3A). This was a tumor-specific finding as increased CD8⁺ T cell frequencies were not observed in the challenge tLN with either treatment compared to control (Figure S3C). This analysis also revealed a comparable reduction in Tregs in challenge tumors from mice treated with α PDL1 or α TGF- β + α PDL1 (Figure 3B), which is consistent with the observed control of challenge tumors. This reduction was specific to Tregs and in the context of the challenge tumor as the frequency of total CD4⁺ T cells in challenge tumors was not different between treatments (Figure S3D) and Tregs were not reduced in challenge tLNs with either treatment (Figure S3E).

To further quantify potential differences in the systemic effects of α PDL1 and α TGF- β + α PDL1 treatment, we next considered more direct measures of systemic anti-tumor immunity. The presence of CD8⁺ T cells specific for p15E, a known murine endogenous retrovirus expressed in MOC1 carcinoma cells,^{18–20} was studied with tetramer staining and flow cytometry. This analysis revealed a greater frequency of p15E-specific CD8⁺ T cells in the spleens of both α PDL1 and α TGF- β + α PDL1 treated mice compared to control, with a greater increase in α TGF- β + α PDL1 treatment mice compared to mice treated with α PDL1 (Figure 3C). Next, splenic CD8⁺ T cells were directly isolated after treatment and assayed for MOC1 tumor specificity in co-culture assays. This analysis revealed a greater number of peripheral CD8⁺ T cells that produced interferon- γ upon exposure to MOC1 tumor cells in both α PDL1 and α TGF- β + α PDL1 treated mice compared to control, with a greater increase in α TGF- β + α PDL1 treatment mice compared to mice treated with α PDL1 (Figure 3D). Finally, the ability of the systemic immune response to directly eliminate adoptively transferred cells pulsed with MOC1 tumor antigen p15E (KSPWF_{TTL}) was measured in an *in vivo* cytotoxicity study (Figure 3E). This highly sensitive, short-term assay revealed greater selective killing of antigen-presenting cells (APCs) pulsed with p15E-peptide and transferred to MOC-1 bearing mice treated with α TGF- β + α PDL1 compared to mice treated with α PDL1 or control (Figures 3F and 3G). Cumulatively, these assays provided multiple independent lines of evidence indicating that although both α PDL1 and α TGF- β + α PDL1 treatment resulted in enhanced systemic anti-tumor immunity compared to control, the magnitude of systemic immunity appears to be greater after α TGF- β + α PDL1 treatment compared to α PDL1 treatment.

Mechanisms underlying the increased primary tumor control observed with the addition of TGF- β neutralization to PDL1 blockade

The primary aim of these studies was to determine alterations in systemic immunity following treatment with α PDL1 and α TGF- β + α PDL1, but we also noted greater primary tumor control with α TGF- β + α PDL1 compared to α PDL1 (as shown in Figure 2B). Interestingly, reduced dose α TGF- β + α PDL1 treatment resulted in control of the primary tumor to a degree similar to that observed with high dose α PDL1 (Figure 4A), indicating that 1/10th of the α TGF- β + α PDL1 treatment dose is similar to full dose α PDL1 alone treatment. Like observations made in challenge tumors, depletion of CD8 cells also abrogated primary tumor growth control observed with α TGF- β + α PDL1 treatment (Figure 4B). However, unlike observations made in challenge tumors, FTY-720 treatment did partially abrogate α TGF- β + α PDL1 treatment-induced primary tumor control (Figure 4C), indicating that trafficking of T cells between the tumor and lymph nodes importantly contributes to local anti-tumor immunity. This observation has been made by others.^{21–24}

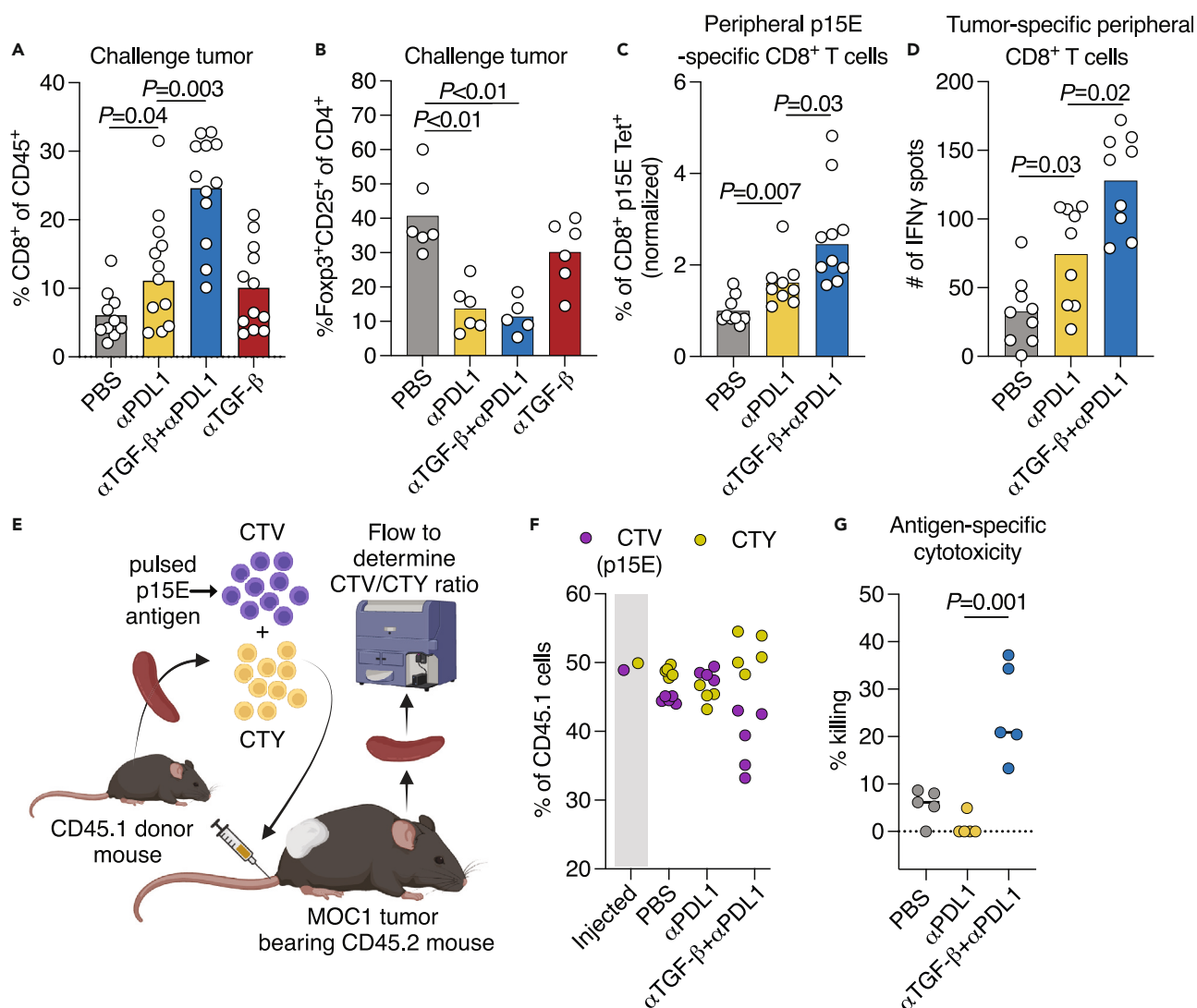


Figure 3. Greater immunity observed with combination PDL1 blockade and TGF- β neutralization using direct measurements of anti-tumor immunity

(A) Bar graph shows the percentage of CD8⁺ cells within the total CD45⁺ compartment in challenge tumors, by treatment. Significance between treatment groups was determined with a Mann-Whitney test. $n = 10$ – 12 mice per treatment group.

(B) Bar graph shows the percentage of Foxp3⁺CD25⁺ cells within the total CD4⁺ compartment in challenge tumors, by treatment. Significance between the treatment groups was determined with a Mann-Whitney test. $n = 5$ – 6 mice per treatment group.

(C) Bar graph shows the percentage of p15E tetramer⁺ cells within the splenic CD8⁺ compartment, by treatment. Spleens were harvested two days after completion of treatment. Significance between the treatment groups was determined with a Mann-Whitney test. $n = 8$ – 10 mice per treatment group.

(D) Bar graph shows the percentage of MOC1 tumor-specific splenic CD8⁺ T cells, by treatment. Spleens were harvested two days after completion of treatment. Significance between the treatment groups was determined with a Mann-Whitney test. $n = 9$ mice per treatment group.

(E) Illustration shows the experimental approach for the *in vivo* cytotoxicity assay.

(F) Dot plot shows the percentage of splenic CD45.1⁺ cells positive for cell trace violet (CTV, loaded with p15E antigen) or cell trace yellow (CTY). Fractions of the cell product prior to adoptive transfer are shown as “Injected.”

(G) Dot plot shows the percentage of selective killing of CTV-labelled (p15E antigen loaded) adoptively transferred cells. Significance between the treatment groups was determined with a Mann-Whitney test. $n = 5$ recipient mice per treatment group.

We next studied how CD8⁺ TIL clonotypes within primary tumors were altered by first focusing on the top 10 most frequent clonotypes within each treatment group. Considering clonotypes with greater than 150 cells as significantly expanded, one clonotype was expanded in the control group (clonotype 3) and one clonotype was expanded in the α TGF- β group (clonotype 6) (Figure 4D). However, 6 clonotypes were expanded in the α PDL1 group and 8 were expanded in the α TGF- β + α PDL1 group. Further, although individual T cell clonotypes were detected in many different transcriptional states (clusters), expanded clonotypes were primarily distributed in the Tex or Tex_{prol} clusters,

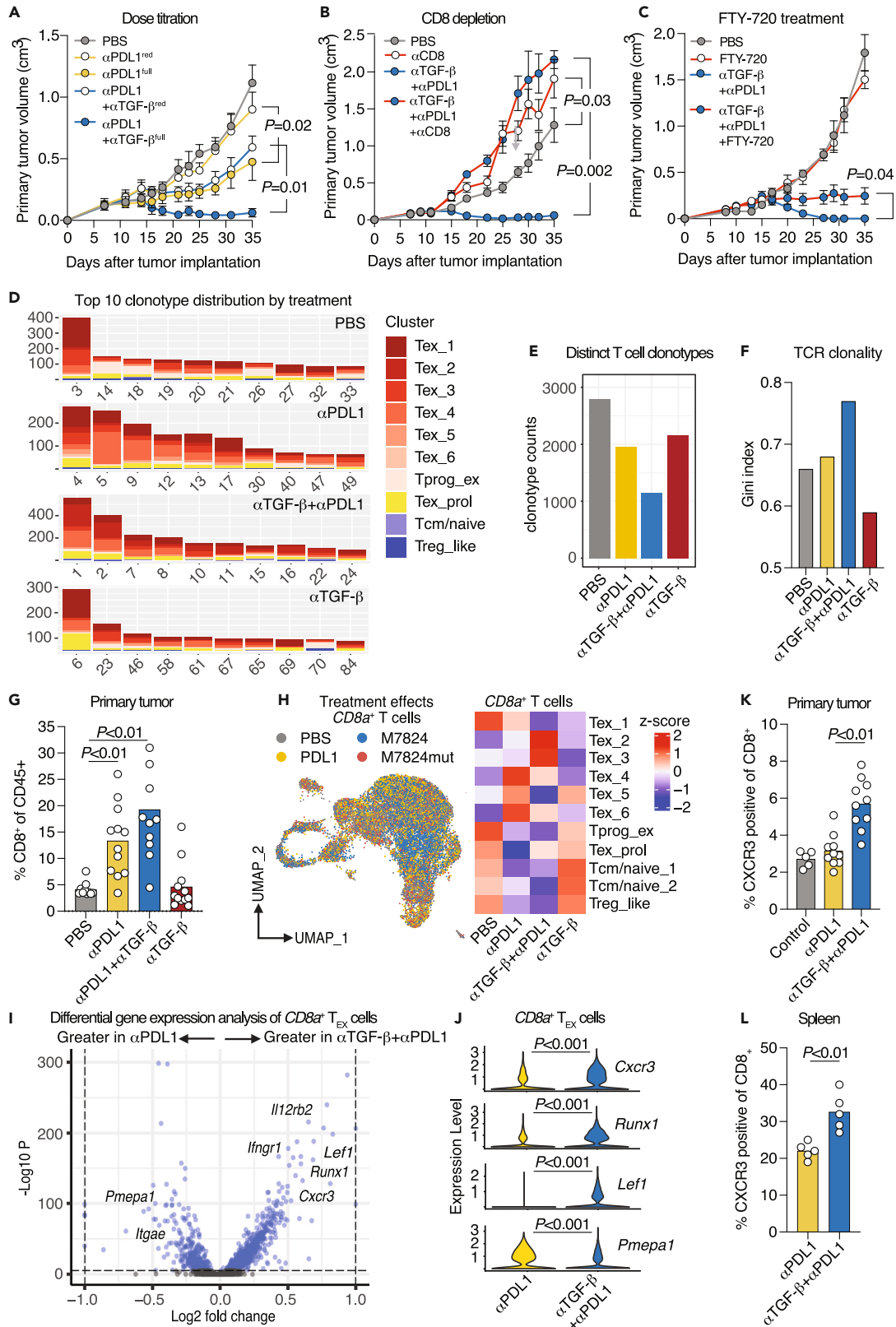


Figure 4. Greater CD8a⁺ T cell clonal expansion and activation in primary tumors observed with combination PDL1 blockade and TGF- β neutralization

- (A) Line graph shows primary tumor growth curves, colored by treatment with either full or reduced dose α PD-L1 or α TGF- β + α PDL1. Significance was determined with one-way ANOVA with multiple comparisons, considering tumor volume from the start of treatment (day 9). $n = 5$ –10 mice per treatment group.
- (B) Line graph shows primary tumor growth curves, colored by treatment with α TGF- β + α PDL1 alone or in combination with CD8 depletion. Significance was determined with one-way ANOVA with multiple comparisons, considering tumor volume from the start of treatment (day 9). $n = 10$ mice per treatment group.
- (C) Line graph shows challenge tumor growth curves, colored by treatment with α TGF- β + α PDL1 alone or in combination with FTY-720. Significance was determined with one-way ANOVA with multiple comparisons, considering tumor volume from the start of treatment (day 9). $n = 5$ mice per treatment group.
- (D) Stacked bar graphs show the cell counts (y axis) and cluster distribution by color of the 10 CD8⁺ TIL clonotypes (x axis) with the greatest frequency within each treatment group.
- (E) Bar graph shows the number of distinct CD8⁺ TIL clonotypes by treatment.
- (F) Bar graph shows the Gini index as a measure of CD8⁺ TIL TCR clonality by treatment.
- (G) Bar graph shows the percentage of CD8⁺ cells within the total CD45 compartment in primary tumors, by treatment. Significance between treatment groups was determined with a Mann-Whitney test. $n = 10$ –12 mice per treatment group.
- (H) Scatterplot shows UMAP embedding of all CD8⁺ TILs, colored by treatment (left) and a heatmap shows the relative frequency of cluster-associated CD8⁺ TILs within the entire CD8⁺ TILs compartment by treatment (right). $n = 5$ mice per treatment group.
- (I) Volcano plot shows the log₂ fold change and significance of differentially expressed genes comparing exhausted CD8⁺ TIL from the α TGF- β + α PDL1 and α PDL1 treatment groups. Significance for each gene is included in the supplemental data file. $n = 5$ mice per treatment group.
- (J) Violin plots show expression of select genes from I. Significance between treatment groups was determined with a Wilcoxon test. $n = 5$ mice per treatment group.
- (K) Bar graph shows the percentage of CXCR3 positive CD8⁺ TILs in primary tumors, by treatment. $n = 10$ mice per treatment group. Significance between treatment groups was determined with a Mann-Whitney test.
- (L) Bar graph shows the percentage of CXCR3 positive CD8⁺ splenic T cells, by treatment. $n = 5$ mice per treatment group. Significance between treatment groups was determined with a Mann-Whitney test.

consistent with human data indicating that primarily exhausted T cell clonotypes expand within the tumor following ICB-based immunotherapy.^{6,8,9} Accordingly, fewer distinct clonotypes (unique TCR sequences) were observed in the α PDL1 and α TGF- β + α PDL1 treated tumors compared to control, with fewer in α TGF- β + α PDL1 treated tumors compared to α PDL1 treated tumors (Figure 4E), providing indirect evidence of clonal expansion. As a more direct measure of TCR clonality, the Gini index was greatest when considering the TCR profile from α TGF- β + α PDL1 treated tumor compared to the other groups (Figure 4F). These data supported that multiple CD8a⁺ TIL clonotypes were expanded in both PDL1 and α TGF- β + α PDL1 treated tumors, but observed expansion of exhausted clonotypes was greater in α TGF- β + α PDL1 compared to α PDL1.

We next studied the CD8⁺ TIL quantity in primary tumors by treatment. Measured by flow cytometry, a greater frequency of CD8⁺ TILs was observed in the α PDL1 and α TGF- β + α PDL1 treatment groups compared to control or α TGF- β although the α PDL1 and α TGF- β + α PDL1 groups were not different from each other (Figure 4G). This was a primary tumor-specific effect since the frequency of CD8⁺ T cells in the primary tdLN following either α PDL1 or α TGF- β + α PDL1 treatment group remained comparable to control (Figure S3F). Given that we observed greater CD8-dependent primary tumor growth control in α TGF- β + α PDL1-treated mice compared to α PDL1-treated mice, but no difference in quantity of CD8⁺ TILs between the α PDL1 and α TGF- β + α PDL1 groups, we next asked if there were differences in cluster distribution or in the CD8a⁺ TIL transcriptional profile after treatment. Treatment with α PDL1 resulted in the relative enrichment of Tex_{4–6} clusters within the total CD8a⁺ TIL compartment, whereas treatment with α TGF- β + α PDL1 resulted in enrichment of clusters Tex₂ and 3 (Figure 4H). Considering differential gene expression analysis between the expanded exhausted clusters following α PDL1 or α TGF- β + α PDL1 treatment, CD8a⁺ TILs from α TGF- β + α PDL1 treated tumors were enriched for expression of genes associated with T cell activation (*Il12rb2* and *Ifngr1*), differentiation/maturation (*Lef1* and *Runx1*) and trafficking (*Cxcr3*) (Figures 4I and 4J). Relative to α PDL1-treated tumors, reduced expression of TGF- β target genes *Itgae* and *Pmepa1* was also observed in α TGF- β + α PDL1-treated CD8a⁺ TILs. Differential gene expression analysis between exhausted CD8a⁺ TIL clusters Tex_{2–6} revealed increased expression of *Cxcr3* in cluster Tex₂, enriched in tumors from mice treated with α TGF- β + α PDL1 relative to α PDL1 (Figure S3G). TGF- β signaling in CD8⁺ T cells reduces expression of CXCR3, resulting in impaired ability of T cells to follow chemokine gradients into tumors.²⁵ Flow cytometry analysis of T cell surface CXCR3 revealed greater expression of CXCR3 on CD8⁺ T cells in the tumor and spleens of mice treated with α TGF- β + α PDL1 compared to mice treated with α PDL1 (Figures 4K and 4L), indicating that TGF- β neutralization can therapeutically enhance CXCR3 expression on T cells. Additionally, compared to *Cxcr3* negative CD8a⁺ T cells in tumors of α TGF- β + α PDL1-treated mice, *Cxcr3* positive CD8a⁺ T cells displayed greater *Cd69*, indicating greater activation, and reduced *Pdcd1*, *Havcr2*, *Lag3*, and *Tox*, indicating reduced exhaustion (Figure S4). Together these data supported that greater CD8⁺ TIL clonal expansion and frequency are observed in primary tumors after treatment with both α PDL1 and α TGF- β + α PDL1. However, relative Tex cluster expansion and gene expression differed between these two treatments, with expansion of Tex clusters expressing greater *Cxcr3* and multiple markers of TIL activation observed to a greater degree in α TGF- β + α PDL1 treated tumors compared to α PDL1.

Given the important roles of CXCR3 in T cell trafficking and function,^{25–27} we next assessed whether our pre-clinical observation of increased T cell CXCR3 expression after α TGF- β + α PDL1 treatment could be made in archived PBMC from patients with newly diagnosed HNSCC treated with α TGF- β + α PDL1 in a previously reported clinical trial^{6,13} (Figure 5A). Flow cytometric analysis revealed consistent and significant increases in cell surface CXCR3 expression on circulating CD8⁺ and CD4⁺ T cells after treatment compared to before (Figures 5B–5D), confirming that the observation of increased CXCR3 expression after TGF- β neutralization and PD-L1 blockade is conserved across murine and human T cells.

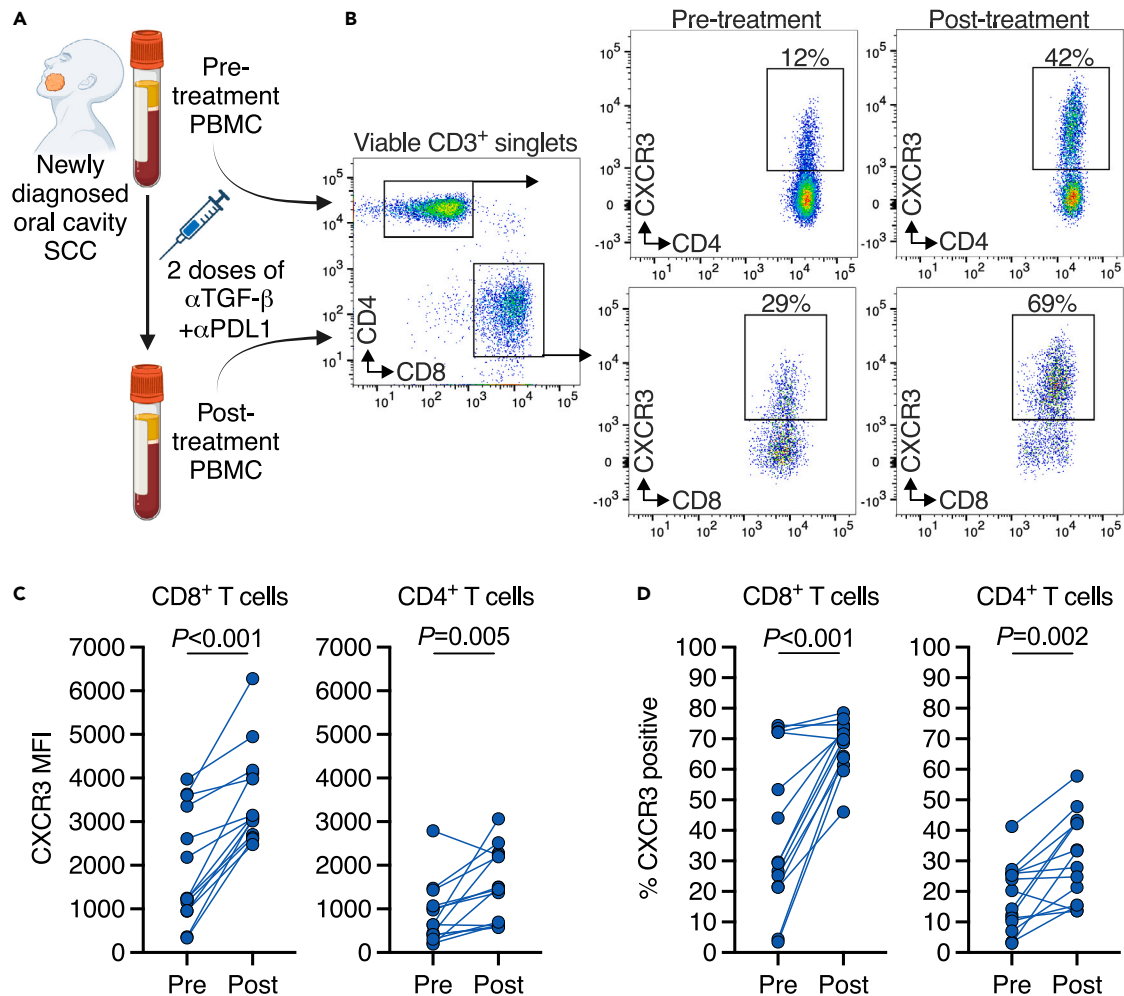


Figure 5. Increased CXCR3 observed on circulating T cells from patients treated with bintrafusp alfa

(A) Illustration shows the collection of PBMC before and after neoadjuvant treatment of patients with newly diagnosed HNSCC with α TGF- β + α PDL1.

(B) Representative flow cytometry dot plots show T cell gating and CXCR3 positive CD8⁺ and CD4⁺ peripheral T cells from patients.

(C and D) Connected line dot plots show flow cytometry quantification of pre- and post-treatment CXCR3 median fluorescent intensity (MFI, C) or percent CXCR3 positivity (D) of CD8⁺ and CD4⁺ peripheral T cells ($n = 14$). Lines connect pre- and post-treatment sample values for individual patients. Significance determined with Wilcoxon matched-pairs signed rank tests.

Finally, possible contributions to the observation of enhanced primary tumor growth control in mice treated with α TGF- β + α PDL1 compared to mice treated with α PDL1 in the CD4⁺ TIL compartment were studied. CD4 depletion totally abrogated α TGF- β + α PDL1-induced primary tumor growth control (Figure 6A), indicating that one or more CD4 populations are required for this therapeutic effect. However, no difference was observed in total CD4⁺ TIL quantity between treatment groups as measured by flow cytometry (Figure 6B). A significant reduction in phosphorylation of SMAD2/3 was observed in CD4⁺ TILs from α TGF- β + α PDL1 treated mice compared to α PDL1 treated mice (Figure 6C), confirming a reduction in signaling downstream of the TGF- β receptor following TGF- β neutralization. Reduced cell surface CD103 expression measured by flow cytometry was also verified on CD4⁺ TILs from mice treated with α TGF- β + α PDL1 compared to mice treated with α PDL1 (Figure 6D). Given that we observed no difference in quantity of CD4⁺ TILs between the α PDL1 and α TGF- β + α PDL1 groups, we next asked if there was a difference in cluster distribution or in the CD4⁺ TIL transcriptional profile after treatment. Relative to α PDL1 treatment, we observed further depletion in Treg clusters Treg_1–3 and an enrichment in the Tex cluster within the total CD4⁺ TIL population after α TGF- β + α PDL1 treatment (Figure 6E). Further study of this Tex cluster revealed a greater T_H1 differentiation score following α TGF- β + α PDL1 treatment compared to α PDL1 treatment (Figure 6F), suggesting that α TGF- β + α PDL1 treatment may polarize non-Treg CD4⁺ helper T cells toward a T_H1 phenotype. Additionally, similar to observations made in the CD8a⁺ TIL compartment, significantly increased *Cxcr3* expression was observed on CD4⁺ TILs after α TGF- β + α PDL1 treatment compared to α PDL1 (Figure 6G). Measuring Tregs in the primary tumor by flow cytometry revealed a reduced frequency of Tregs in both the α PDL1 and α TGF- β + α PDL1 treatment groups compared to control or α TGF- β , although the α PDL1 and α TGF- β + α PDL1 groups were not different from each other (Figure 6H). This

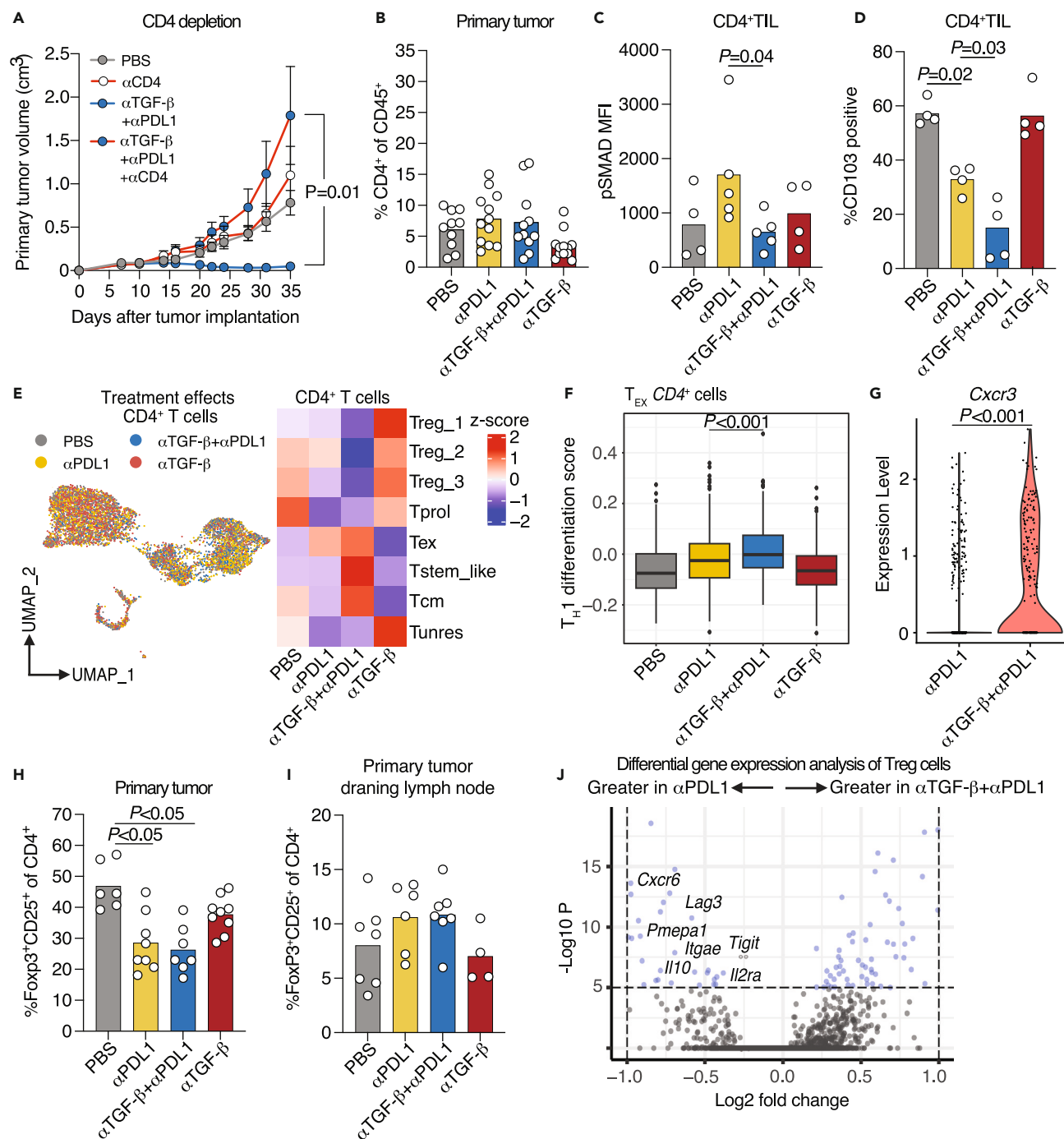


Figure 6. Greater CD4⁺ T_H1 polarization and Treg alterations in primary tumors observed with combination PDL1 blockade and TGF- β neutralization

(A) Line graph shows primary tumor growth curves, colored by treatment with α TGF- β + α PDL1 alone or in combination with CD4 depletion. Significance was determined with one-way ANOVA with multiple comparisons, considering tumor volume from the start of treatment (day 9). $n = 10$ mice per treatment group. (B) Bar graph shows the percentage of CD4⁺ cells within the total CD45 compartment in primary tumors, by treatment. Significance between treatment groups was determined with a Mann-Whitney test. $n = 10$ –11 mice per treatment group. (C) Bar graph shows the mean fluorescence intensity (MFI) of pSMAD expression in CD4⁺ TILs measured by flow cytometry. $n = 4$ –5 mice per treatment group. Significance between treatment groups was determined with a Mann-Whitney test. (D) Bar graph shows CD103 expression on CD4⁺ TILs measured by flow cytometry. $n = 4$ mice per treatment group. Significance between treatment groups was determined with a Mann-Whitney test.

Figure 6. Continued

- (E) Scatterplot shows UMAP embedding of all $CD4^+$ TILs, colored by treatment (left) and a heatmap showing the relative frequency of cluster-associated $CD4^+$ TILs within the entire $CD4^+$ TIL compartment by treatment (right). $n = 5$ mice per treatment group.
- (F) Box and whisker plot shows the Reactome T_H1 differentiation score within the $CD4^+$ T_{EX} cluster by treatment. Significance between treatment groups was determined with a Wilcoxon test. $n = 5$ mice per treatment group.
- (G) Violin plot shows *Cxcr3* expression on $CD4^+$ T cells from the Tex cluster by treatment group. Significance between treatment groups was determined with a Wilcoxon test. $n = 5$ mice per treatment group.
- (H) Bar graph shows the percentage of $FoxP3^+CD25^+$ cells within the total CD4 compartment in primary tumors, by treatment. Significance between the treatment groups was determined with a Mann-Whitney test. $n = 6-8$ mice per treatment group.
- (I) Bar graph shows the percentage of $FoxP3^+CD25^+$ cells within the total CD4 compartment in the tdLN, by treatment. Significance between the treatment groups was determined with a Mann-Whitney test. $n = 6-8$ mice per treatment group.
- (J) Volcano plot shows the log₂ fold change and significance of differentially expressed genes comparing $FoxP3^+CD25^+CD4^+$ TIL (Treg clusters 1–3 considered together) from the α TGF- β + α PDL1 and α PDL1 treatment groups. Significance for each gene is included in the supplemental data file. $n = 5$ mice per treatment group.

Treg reduction following both treatments was a primary tumor-specific effect since the frequency of Tregs cells in the primary tdLN was not reduced compared to control (Figure 6I). Given that we observed no difference in quantity of primary tumor Tregs between the α PDL1 and α TGF- β + α PDL1 groups, we next asked if there were differentially expressed genes that may indicate differential function. We observed a relative enrichment of multiple Treg function (*Il2ra* and *Cxcr6*) and immunosuppressive genes (*Il10*, *Tigit*, and *Lag3*) in the PDL1 treated Tregs, indicating a relative reduction in expression of these genes in Tregs following α TGF- β + α PDL1 treatment (Figure 6J). These data supported that greater polarization toward T_H1 helper function in non-Treg $CD4^+$ TILs and reduced immunosuppressive capacity of Tregs may contribute to the observation of enhanced primary tumor control in mice treated with α TGF- β + α PDL1 compared to mice treated with α PDL1.

DISCUSSION

In patients with HNSCC, greater recurrence free survival (RFS) compared to historical controls is observed in multiple phase II studies of neoadjuvant ICB immunotherapy. Multiple recent reports have also indicated that either ICB alone or in combination with TGF- β neutralization results in the apparent egress of tumor-specific T cells from tissue and into circulation.^{6,8} Mechanistic association between this enhanced frequency of tumor-specific T cells in circulation and improved RFS survival after neoadjuvant immunotherapy is needed, but this association is a rationale hypothesis as pre-clinical studies have demonstrated that tumor-specific T cells in circulation can eliminate disseminated tumor cells and micrometastases.^{28–30} Here, using multiple independent genomic and functional experimental techniques, we experimentally validated that movement of exhausted TILs into circulation results in enhanced systemic anti-tumor immunity. We evaluated if the addition of TGF- β neutralization enhanced systemic anti-tumor immunity beyond that observed with PDL1 ICB alone. Our findings demonstrate that the addition of TGF- β neutralization to PDL1 ICB resulted in greater detection of exhausted TILs in circulation and greater functional systemic anti-tumor immunity compared to ICB alone. If a goal of neoadjuvant treatment is to induce egress of as many tumor-specific T cells as possible out of the immunosuppressive TME into circulation prior to surgical removal of these tissues, then the addition of TGF- β neutralization to ICB achieves this goal better than ICB alone.

CD103 is a TGF- β -responsive integrin that binds E-cadherin and contributes to the adhesion and tissue retention of T cells that have assumed a tissue resident-like phenotype. One mechanism underlying the enhanced tissue egress and systemic anti-tumor immunity observed following TGF- β neutralization plus ICB treatment appeared to be a reduction in $CD8^+$ TIL CD103 expression. This was also observed in HNSCC patients treated with neoadjuvant bintrafusp alfa.⁶ Following TGF- β neutralization, we observed reduced expression of *Znf683*, the gene that encodes the transcription factor Hobit. Hobit serves as a core transcriptional regulator of the tissue resident phenotype in T cells³¹ and a direct relationship between TGF- β signaling and Hobit expression in T cells has been reported.³² Expression of Hobit may also identify $CD8^+$ TILs that mediate immune-related pathologic tumor responses in HNSCC patients receiving neoadjuvant ICB,⁹ further inferring the possible tumor-specificity of Hobit⁺ $CD8^+$ TILs.

We observed increased frequencies of splenic TCRs associated with exhausted TILs following α PDL1 or α TGF- β + α PDL1 treatment, but no association between exhausted TILs and TCRs from tdLNs. Combined with our observation that treatment with the LN-egress inhibitor FTY-720 did not alter the ability of α TGF- β + α PDL1 treatment to induce strong systemic anti-tumor immunity, these data suggested that the origin of the tumor-specific T cells in circulation that mediate enhanced systemic anti-tumor immunity is most likely the primary tumor. Our data indicate that trafficking of tumor-specific T cells between the tdLN and primary tumor is important for effective ICB immunotherapy-induced primary tumor control; an observation previously made by others.^{21–24} Understanding if circulating $CD8^+$ T cells with tumor-specificity originate exclusively from the primary tumor or if the tdLN also contributes to this effect is relevant for complete mechanistic understanding of the treatment and how it promotes enhanced systemic anti-tumor immunity. Translationally, however, understanding whether it is important to administer neoadjuvant or induction immunotherapy prior to surgical removal or irradiation of the primary tumor or tdLN may be less significant as definitive treatment of newly diagnosed HNSCC often includes surgical removal or irradiation of both the primary tumor and tdLN.

The addition of TGF- β neutralization to ICB also appeared to increase $CD8^+$ T cell expression of CXCR3, the cognate receptor for the T cell chemokines CXCL9, CXCL10, and CXCL11,²⁶ compared to ICB alone. This observation was also validated in archived PBMC samples from a previously reported prospective trial of patients with newly diagnosed HNSCC treated with bintrafusp alfa. CXCR3 directs the migration of T cells into solid tumors and may facilitate T cell and dendritic cell interactions in the TME.^{25–27} Increased CXCR3 expression may underlie the

observation of increased trafficking of CD8⁺ T cells into challenge tumors of mice treated with α TGF- β + α PDL1 compared to mice treated with PDL1 alone. TGF- β signaling in T cells is known to drive a reduction in CXCR3.²⁵ Our results extend these mechanistic findings and suggest that therapeutic inhibition of TGF- β may facilitate improved T cell tumor trafficking and function through manipulation of CXCR3 expression.

We also observed greater primary tumor control with the addition of TGF- β neutralization to ICB. This has previously been observed¹⁵ and reviewed.³³ Our observations indicate that increased CD8⁺ TIL clonal expansion and activation, helper CD4⁺ TIL T_H1 polarization, and reduced Treg number and immunosuppressive function in tumors treated with TGF- β neutralization in addition to ICB may all play a mechanistic role.

Overall, our results provide a scientific rationale for the continued clinical study of ICB plus TGF- β neutralization in the neoadjuvant setting in patients with newly diagnosed HNSCC. The goal of immunotherapy in the neoadjuvant clinical setting is to enhance the systemic anti-tumor immunity that will remain in patients following resection of locoregional disease. This mechanistic goal of treatment may be unique to the neoadjuvant clinical setting, as egress of tumor-specific TILs from the tumor into circulation may not necessarily be the goal of treatment in the setting of disease that is not going to be surgically removed. Our team observed greater than expected RFS compared to historical controls and enhanced post-treatment systemic anti-tumor immunity in a neoadjuvant study of bintrafusp alfa in patients with newly diagnosed HNSCC.^{6,13} However, study of this agent in patients with unresectable locoregionally advanced or metastatic non-small cell lung cancer (NSCLC) not treated with surgery revealed no improvement in progression-free survival over PD-1 ICB.³⁴ One possible explanation for the differential observation is that the clinical benefit of adding TGF- β neutralization to ICB may be dependent on the tumor itself and the particular clinical setting, and perhaps more importantly, a reflection of the biologic role of TGF- β in individual tumor types.³⁵

In conclusion, our results demonstrate that egress of exhausted CD8⁺ TILs from tumors into circulation after immunotherapy results in enhanced systemic anti-tumor immunity. Treatment with PDL1 alone or in combination with TGF- β neutralization enhances systemic anti-tumor immunity, but the magnitude of this response is greater with the addition of TGF- β neutralization. Egress of exhausted CD8⁺ TILs from tumors into circulation and enhanced systemic immunity associate with reductions in Hobit and CD103 expression, indicating partial reversal of a tissue resident-like CD8⁺ TIL phenotype following TGF- β neutralization. Additionally, enhanced T cell CXCR3 expression in our mouse model after α TGF- β + α PDL1 treatment and in human HNSCC-patient's PBMC samples after bintrafusp alfa treatment provides a potential direct link between TGF- β neutralization and enhanced T cell function and tumor trafficking. Clinically, the need to balance the possible increased benefit from enhanced systemic anti-tumor immunity with the possible increased toxicity from the addition of TGF- β blockade to ICB exists. However, our results show that α TGF- β + α PDL1 enhances systemic immunity against solid tumors and provide the scientific rationale to add TGF- β blockade to ICB in the treatment of patients with newly diagnosed carcinomas prior to definitive treatment.

Limitations of the study

Limitations of this study exist. We used a single syngeneic mouse model to study differences in systemic anti-tumor immunity between multiple treatments. Even though increased circulation of tumor-specific T cells in patients with HNSCC treated with bintrafusp alfa had already been observed,⁶ similar pre-clinical findings as those described here across multiple syngeneic models would more strongly imply generalizability. We chose to work exclusively with the MOC1 model as it does not generate systemic immunity of sufficient magnitude to reject a challenge tumor in the absence of immunotherapy,¹⁸ making it ideal to study the ability of different immunotherapies to increase systemic anti-tumor immunity. Our studies also do not address the durability of the enhanced systemic anti-tumor immunity observed after treatment. This would require similar tumor challenge and functional immune assays to be performed at multiple time points after completion of treatment. Additionally, although multiple independent assays infer that enhanced systemic anti-tumor immunity results in rejection of contralateral challenge tumors after treatment, analysis of shared TCR repertoires between primary and secondary tumors in individual mice would be needed to definitively demonstrate that T cell clones from the primary tumor moved through circulation and into secondary tumors. These analyses were not performed.

STAR★METHODS

Detailed methods are provided in the online version of this paper and include the following:

- KEY RESOURCES TABLE
- RESOURCE AVAILABILITY
 - Lead contact
 - Materials availability
 - Data and code availability
- EXPERIMENTAL MODEL AND STUDY PARTICIPANT DETAILS
 - Animals
 - Human participants
 - Cell lines
- METHOD DETAILS
 - Reagents
 - Murine studies
 - Histologic analysis

- T cell sorting from tumors and single-cell RNA- and TCR-sequencing
- T cell sorting from spleens and lymph nodes and deep TCR sequencing
- Bioinformatic analysis
- Flow cytometry
- *In vitro* T cell studies
- *In vivo* cytotoxicity assay
- Peripheral T cell tumor-specificity assay
- **QUANTIFICATION AND STATISTICAL ANALYSIS**
- **ADDITIONAL RESOURCES**

SUPPLEMENTAL INFORMATION

Supplemental information can be found online at <https://doi.org/10.1016/j.isci.2024.110520>.

ACKNOWLEDGMENTS

Research support was provided by the Intramural Research Program of the National Cancer Institute (project number ZIA BC012131) and the NIH Medical Research Scholars Program, a public-private partnership supported jointly by the NIH and contributions to the Foundation for the NIH from the American Association for Dental Research and the Colgate-Palmolive Company. This work utilized the computational resources of the NIH HPC Biowulf cluster (<http://hpc.nih.gov>). The authors thank Dr. Xiaolin Wu, Genomics Core, Center for Cancer Research, NCI for RNA-sequencing support and Dr. Christopher Silvin for cell sorting support. Figure illustrations were generated using Biorender (www.biorender.com). The healthcare business of Merck KGaA, Darmstadt, Germany (CrossRef Funder ID: 10.13039/100009945) reviewed this manuscript for medical accuracy only before journal submission. The authors are fully responsible for the content of this manuscript, and the views and opinions described in the publication reflect solely those of the authors.

AUTHOR CONTRIBUTIONS

Conceptualization, C.T.A. and M.C.; methodology, C.T.A. and M.C.; investigation, M.F., C.S., Y.R., X.Y., A.H., C.T.A., and M.C.; writing – original draft, M.F. and M.C.; writing – review & editing, M.F., C.S., Y.R., X.Y., A.H., J.M.R., J.W.H., J.S., J.L.G., C.T.A., and M.C.; funding acquisition, C.T.A.; resources, J.M.R., J.W.H., J.S., J.L.G., and C.T.A.; supervision, J.W.H., J.S., J.L.G., C.T.A., and M.C.

DECLARATION OF INTERESTS

The authors declare no competing interests.

Received: February 8, 2024

Revised: June 27, 2024

Accepted: July 12, 2024

Published: July 15, 2024

REFERENCES

1. Tumeah, P.C., Harview, C.L., Yearley, J.H., Shintaku, I.P., Taylor, E.J., Robert, L., Chmielowski, B., Spasic, M., Henry, G., Ciobanu, V., et al. (2014). PD-1 blockade induces responses by inhibiting adaptive immune resistance. *Nature* 515, 568–571. <https://doi.org/10.1038/nature13954>.
2. Daniel, B., Yost, K.E., Hsiung, S., Sandor, K., Xia, Y., Qi, Y., Hiam-Galvez, K.J., Black, M., C, J.R., Shi, Q., et al. (2022). Divergent clonal differentiation trajectories of T cell exhaustion. *Nat. Immunol.* 23, 1614–1627. <https://doi.org/10.1038/s41590-022-01337-5>.
3. Gavil, N.V., Scott, M.C., Weyu, E., Smith, O.C., O’Flanagan, S.D., Wijeyesinghe, S., Lotfi-Emran, S., Shiao, S.L., Vezys, V., and Masopust, D. (2023). Chronic antigen in solid tumors drives a distinct program of T cell residence. *Sci. Immunol.* 8, eadd5976. <https://doi.org/10.1126/sciimmunol.add5976>.
4. Christo, S.N., Evrard, M., Park, S.L., Gandolfo, L.C., Burn, T.N., Fonseca, R., Newman, D.M., Alexandre, Y.O., Collins, N., Zamudio, N.M., et al. (2021). Discrete tissue microenvironments instruct diversity in resident memory T cell function and plasticity. *Nat. Immunol.* 22, 1140–1151. <https://doi.org/10.1038/s41590-021-01004-1>.
5. Duhon, T., Duhon, R., Montler, R., Moses, J., Moudgil, T., de Miranda, N.F., Goodall, C.P., Blair, T.C., Fox, B.A., McDermott, J.E., et al. (2018). Co-expression of CD39 and CD103 identifies tumor-reactive CD8 T cells in human solid tumors. *Nat. Commun.* 9, 2724. <https://doi.org/10.1038/s41467-018-05072-0>.
6. Sievers, C., Craveiro, M., Friedman, J., Robbins, Y., Yang, X., Bai, K., Nguyen, A., Redman, J.M., Chari, R., Soon-Shiong, P., et al. (2023). Phenotypic plasticity and reduced tissue retention of exhausted tumor-infiltrating T cells following neoadjuvant immunotherapy in head and neck cancer. *Cancer Cell* 41, 887–902.e5. <https://doi.org/10.1016/j.ccell.2023.03.014>.
7. Sade-Feldman, M., Yizhak, K., Bjorgaard, S.L., Ray, J.P., de Boer, C.G., Jenkins, R.W., Lieb, D.J., Chen, J.H., Frederick, D.T., Barzily-Rokni, M., et al. (2018). Defining T Cell States Associated with Response to Checkpoint Immunotherapy in Melanoma. *Cell* 175, 998–1013.e20. <https://doi.org/10.1016/j.cell.2018.10.038>.
8. Luoma, A.M., Suo, S., Wang, Y., Gunasti, L., Porter, C.B.M., Nabils, N., Tadros, J., Ferretti, A.P., Liao, S., Gurer, C., et al. (2022). Tissue-resident memory and circulating T cells are early responders to pre-surgical cancer immunotherapy. *Cell* 185, 2918–2935.e29. <https://doi.org/10.1016/j.cell.2022.06.018>.
9. Oliveira, G., Egloff, A.M., Afeyan, A.B., Wolff, J.O., Zeng, Z., Chernock, R.D., Zhou, L., Messier, C., Lizotte, P., Pfaff, K.L., et al. (2023). Preexisting tumor-resident T cells with cytotoxic potential associate with response to neoadjuvant anti-PD-1 in head and neck cancer. *Sci. Immunol.* 8, eadf4968. <https://doi.org/10.1126/sciimmunol.adf4968>.
10. Virassamy, B., Caramia, F., Savas, P., Sant, S., Wang, J., Christo, S.N., Byrne, A., Clarke, K., Brown, E., Teo, Z.L., et al. (2023). Intratumoral CD8(+) T cells with a tissue-resident memory phenotype mediate local immunity and immune checkpoint responses in breast

- cancer. *Cancer Cell* 41, 585–601.e8. <https://doi.org/10.1016/j.ccell.2023.01.004>.
11. Chow, L.Q.M. (2020). Head and Neck Cancer. *N. Engl. J. Med.* 382, 60–72. <https://doi.org/10.1056/NEJMra1715715>.
 12. Rainey, M.A., Allen, C.T., and Craveiro, M. (2023). Egress of resident memory T cells from tissue with neoadjuvant immunotherapy: Implications for systemic anti-tumor immunity. *Oral Oncol.* 146, 106570. <https://doi.org/10.1016/j.oraloncology.2023.106570>.
 13. Redman, J.M., Friedman, J., Robbins, Y., Sievers, C., Yang, X., Lassoued, W., Sinkoe, A., Papanicolau-Sengos, A., Lee, C.C., Marte, J.L., et al. (2022). Enhanced neoepitope-specific immunity following neoadjuvant PD-L1 and TGF- β blockade in HPV-unrelated head and neck cancer. *J. Clin. Invest.* 132, e161400. <https://doi.org/10.1172/JCI161400>.
 14. Onken, M.D., Winkler, A.E., Kanchi, K.L., Chalivendra, V., Law, J.H., Rickert, C.G., Kallogjeri, D., Judd, N.P., Dunn, G.P., Piccirillo, J.F., et al. (2014). A surprising cross-species conservation in the genomic landscape of mouse and human oral cancer identifies a transcriptional signature predicting metastatic disease. *Clin. Cancer Res.* 20, 2873–2884. <https://doi.org/10.1158/1078-0432.CCR-14-0205>.
 15. Lan, Y., Zhang, D., Xu, C., Hance, K.W., Marelli, B., Qi, J., Yu, H., Qin, G., Sircar, A., Hernandez, V.M., et al. (2018). Enhanced preclinical antitumor activity of M7824, a bifunctional fusion protein simultaneously targeting PD-L1 and TGF- β . *Sci. Transl. Med.* 10, eaan5488. <https://doi.org/10.1126/scitranslmed.aan5488>.
 16. Lowery, F.J., Krishna, S., Yossef, R., Parikh, N.B., Chatani, P.D., Zacharakis, N., Parkhurst, M.R., Levin, N., Sindiri, S., Sachs, A., et al. (2022). Molecular signatures of antitumor neoantigen-reactive T cells from metastatic human cancers. *Science* 375, 877–884. <https://doi.org/10.1126/science.abl5447>.
 17. Oliveira, G., Stromhaug, K., Klaeger, S., Kula, T., Frederick, D.T., Le, P.M., Forman, J., Huang, T., Li, S., Zhang, W., et al. (2021). Phenotype, specificity and avidity of antitumor CD8(+) T cells in melanoma. *Nature* 596, 119–125. <https://doi.org/10.1038/s41586-021-03704-y>.
 18. Friedman, J., Moore, E.C., Zolkind, P., Robbins, Y., Clavijo, P.E., Sun, L., Greene, S., Morisada, M.V., Mydlarz, W.K., Schmitt, N., et al. (2020). Neoadjuvant PD-1 Immune Checkpoint Blockade Reverses Functional Immunodominance among Tumor Antigen-Specific T Cells. *Clin. Cancer Res.* 26, 679–689. <https://doi.org/10.1158/1078-0432.CCR-19-2209>.
 19. Nagaya, T., Friedman, J., Maruoka, Y., Ogata, F., Okuyama, S., Clavijo, P.E., Choyke, P.L., Allen, C., and Kobayashi, H. (2019). Host Immunity Following Near-Infrared Photoimmunotherapy Is Enhanced with PD-1 Checkpoint Blockade to Eradicate Established Antigenic Tumors. *Cancer Immunol. Res.* 7, 401–413. <https://doi.org/10.1158/2326-6066.CIR-18-0546>.
 20. Moore, E.C., Cash, H.A., Caruso, A.M., Uppaluri, R., Hodge, J.W., Van Waes, C., and Allen, C.T. (2016). Enhanced Tumor Control with Combination mTOR and PD-L1 Inhibition in Syngeneic Oral Cavity Cancers. *Cancer Immunol. Res.* 4, 611–620. <https://doi.org/10.1158/2326-6066.CIR-15-0252>.
 21. Fransen, M.F., Schoonderwoerd, M., Knopf, P., Camps, M.G., Hawinkels, L.J., Kneilling, M., van Hall, T., and Ossendorp, F. (2018). Tumor-draining lymph nodes are pivotal in PD-1/PD-L1 checkpoint therapy. *JCI Insight* 3, e124507. <https://doi.org/10.1172/jci.insight.124507>.
 22. Saddawi-Konefka, R., O'Farrell, A., Faraji, F., Clubb, L., Allevato, M.M., Jensen, S.M., Yung, B.S., Wang, Z., Wu, V.H., Anang, N.A., et al. (2022). Lymphatic-preserving treatment sequencing with immune checkpoint inhibition unleashes cDC1-dependent antitumor immunity in HNSCC. *Nat. Commun.* 13, 4298. <https://doi.org/10.1038/s41467-022-31941-w>.
 23. Darragh, L.B., Gadwa, J., Pham, T.T., Van Court, B., Neupert, B., Olimpo, N.A., Nguyen, K., Nguyen, D., Knitz, M.W., Hoen, M., et al. (2022). Elective nodal irradiation mitigates local and systemic immunity generated by combination radiation and immunotherapy in head and neck tumors. *Nat. Commun.* 13, 7015. <https://doi.org/10.1038/s41467-022-34676-w>.
 24. Li, Z., Tuong, Z.K., Dean, I., Willis, C., Gaspar, F., Fiancette, R., Idris, S., Ghanem, B., Ferdinand, J.R., Penalver, A., et al. (2022). In vivo labeling reveals continuous trafficking of TCF-1+ T cells between tumor and lymphoid tissue. *J. Exp. Med.* 219, e20210749. <https://doi.org/10.1084/jem.20210749>.
 25. Gunderson, A.J., Yamazaki, T., McCarty, K., Fox, N., Phillips, M., Alice, A., Blair, T., Whiteford, M., O'Brien, D., Ahmad, R., et al. (2020). TGF β suppresses CD8⁺ T cell expression of CXCR3 and tumor trafficking. *Nat. Commun.* 11, 1749. <https://doi.org/10.1038/s41467-020-15404-8>.
 26. Chheda, Z.S., Sharma, R.K., Jala, V.R., Luster, A.D., and Haribabu, B. (2016). Chemoattractant Receptors BLT1 and CXCR3 Regulate Antitumor Immunity by Facilitating CD8+ T Cell Migration into Tumors. *J. Immunol.* 197, 2016–2026. <https://doi.org/10.4049/jimmunol.1502376>.
 27. Chow, M.T., Ozga, A.J., Servis, R.L., Frederick, D.T., Lo, J.A., Fisher, D.E., Freeman, G.J., Boland, G.M., and Luster, A.D. (2019). Intratumoral Activity of the CXCR3 Chemokine System Is Required for the Efficacy of Anti-PD-1 Therapy. *Immunity* 50, 1498–1512.e5. <https://doi.org/10.1016/j.immuni.2019.04.010>.
 28. Piranlioglu, R., Lee, E., Ouzounova, M., Bollag, R.J., Vinyard, A.H., Arbab, A.S., Marasco, D., Guzel, M., Cowell, J.K., Thangaraju, M., et al. (2019). Primary tumor-induced immunity eradicates disseminated tumor cells in syngeneic mouse model. *Nat. Commun.* 10, 1430. <https://doi.org/10.1038/s41467-019-09015-1>.
 29. Schirmacher, V., von Hoegen, P., Griesbach, A., Schild, H.J., and Zangemeister-Wittke, U. (1991). Specific eradication of micrometastases by transfer of tumour-immune T cells from major-histocompatibility-complex congenic mice. *Cancer Immunol. Immunother.* 32, 373–381. <https://doi.org/10.1007/BF01741332>.
 30. Koebel, C.M., Vermi, W., Swann, J.B., Zerafa, N., Rodig, S.J., Old, L.J., Smyth, M.J., and Schreiber, R.D. (2007). Adaptive immunity maintains occult cancer in an equilibrium state. *Nature* 450, 903–907. <https://doi.org/10.1038/nature06309>.
 31. Mackay, L.K., Minnich, M., Kragten, N.A., Liao, Y., Nota, B., Seillet, C., Zaid, A., Man, K., Preston, S., Freestone, D., et al. (2016). Hobit and Blimp1 instruct a universal transcriptional program of tissue residency in lymphocytes. *Science* 352, 459–463. <https://doi.org/10.1126/science.aad2035>.
 32. Chandiran, K., Suarez-Ramirez, J.E., Hu, Y., Jellison, E.R., Ugr, Z., Low, J.S., McDonald, B., Kaech, S.M., and Cauley, L.S. (2022). SMAD4 and TGF β are architects of inverse genetic programs during fate determination of antiviral CTLs. *Elife* 11, e76457. <https://doi.org/10.7554/eLife.76457>.
 33. Lind, H., Gameiro, S.R., Jochems, C., Donahue, R.N., Strauss, J., Gulley, J.M., Palena, C., and Schlom, J. (2020). Dual targeting of TGF- β and PD-L1 via a bifunctional anti-PD-L1/TGF- β RII agent: status of preclinical and clinical advances. *J. Immunother. Cancer* 8, e000433. <https://doi.org/10.1136/jitc-2019-000433>.
 34. Cho, B.C., Lee, J.S., Wu, Y.L., Cicin, I., Dols, M.C., Ahn, M.J., Cuppens, K., Veillon, R., Nadal, E., Dias, J.M., et al. (2023). Bintrafusp Alfa Versus Pembrolizumab in Patients With Treatment-Naive, Programmed Death-Ligand 1-High Advanced NSCLC: A Randomized, Open-Label, Phase 3 Trial. *J. Thorac. Oncol.* 18, 1731–1742. <https://doi.org/10.1016/j.jtho.2023.08.018>.
 35. Batlle, E., and Massague, J. (2019). Transforming Growth Factor- β Signaling in Immunity and Cancer. *Immunity* 50, 924–940. <https://doi.org/10.1016/j.immuni.2019.03.024>.
 36. Hong, Y., Robbins, Y., Yang, X., Mydlarz, W.K., Sowers, A., Mitchell, J.B., Gulley, J.L., Schlom, J., Gameiro, S.R., Sievers, C., and Allen, C.T. (2022). Cure of syngeneic carcinomas with targeted IL-12 through obligate reprogramming of lymphoid and myeloid immunity. *JCI Insight* 7, e157448. <https://doi.org/10.1172/jci.insight.157448>.
 37. Sievers, C., Robbins, Y., Bai, K., Yang, X., Clavijo, P.E., Friedman, J., Sinkoe, A., Norberg, S.M., Hinrichs, C., Van Waes, C., and Allen, C.T. (2021). Comprehensive multiomic characterization of human papillomavirus-driven recurrent respiratory papillomatosis reveals distinct molecular subtypes. *Commun. Biol.* 4, 1416. <https://doi.org/10.1038/s42003-021-02942-0>.
 38. Barcelo, H., Faul, J., Crimmins, E., and Thyagarajan, B. (2018). A Practical Cryopreservation and Staining Protocol for Immunophenotyping in Population Studies. *Curr. Protoc. Cytom.* 84, e35. <https://doi.org/10.1002/cpcy.35>.

STAR★METHODS

KEY RESOURCES TABLE

REAGENT or RESOURCE	SOURCE	IDENTIFIER
Antibodies		
CD4 (GK1.5)	Biolegend	100422; RRID: AB_312706
CD8 (53-6.7)	BD Biosciences	100711; RRID: AB_312750
CD8	MBL International	753756; RRID: AB_469584
CD16/32 (2.4G2)	Tonbo/Cytek Biosciences	70-0161-U500; RRID: AB_2621487
CD25 (3C7)	Biolegend	101918; RRID: AB_2650981
CD45 (30-F11)	Biolegend	103112; RRID: AB_312976
C45.1 (A20)	Biolegend	110720; RRID: AB_492864
CD103 (2E7)	Biolegend	121430; RRID: AB_2566492
CXCR3 (173)	Biolegend	126536; RRID: AB_2566564
Foxp3 (MF-14)	Biolegend	126410; RRID: AB_2247064
TCR-β (H57-597)	Biolegend	109226; RRID: AB_1027655
p15E:H-2Kb tetramer	MBL International	TB-M507-2
CD3 (OKT3)	Biolegend	317314; RRID: AB_571908
CD4 (OKT4)	Biolegend	317413; RRID: AB_571958
CD8 (SK1)	BD Biosciences	753756; RRID: AB_467092
CXCR3 (G025H7)	Biolegend	126536; RRID: AB_2566564
Anti-wide spectrum Cytokeratin	Abcam	AB9377; RRID: AB_307222
Biological samples		
Archived human PBMC	Clinical trial	NCT04247282
Chemicals, peptides, and recombinant proteins		
Recombinant Mouse TGF-β1	Biolegend	763104
GhostDye Violet510	Tonbo/Cytek Biosciences	13-0870-T500
PFA solution in PBS 4%	USB Corporation	199431LT
Methanol	Sigma Aldrich	34860-1L-R
SytoxGreen	Thermo Fisher Scientific	S34860
Cell Trace Violet	Thermo Fisher Scientific	C34557
Cell Trace Yellow	Thermo Fisher Scientific	C34573
eBioscience Cell Stimulation Cocktail	Thermo Fisher Scientific	00-4970-93
Foxp3/Transcription Factor Staining Buffer Set	Thermo Fisher Scientific	00-5523-00
Bovine Serum Albumin	Sigma Aldrich	A9647-500G
FTY720	Sigma Aldrich	SML0700-5MG
Sodium Azide	Sigma Aldrich	S2002-100G
RPMI-1640	Cytiva	SH30027.01
PBS 1x	Crystalgen	221-132-10
ACK lysis buffer	Quality Biological	118-156-721
CTS AIM V Medium	Gibco	0870112-DK
Gentamicin	Gibco	15710-064
L-Glutamine 200mM (100x)	Gibco	25030-081
Pen Strep	Gibco	15140-148
FBS	Gibco	16000-044

(Continued on next page)

Continued

REAGENT or RESOURCE	SOURCE	IDENTIFIER
Hepes Buffer	Corning	25-060-CI
Matrigel	R&D Systems	3632-005-02
Avelumab (α PDL1)	Merck KGaA	MSB0010718C
Bintrafusp alfa (α TGF- β + α PDL1)	EMD Serono	MSB0011359C
α TGF- β + α PDL1mut	EMD Serono	https://doi.org/10.13039/100004755
Human Serum AB	GeminiBio	100-512

Critical commercial assays

Mouse IFN-gamma ELISpot Kit	R&D Systems	XEL485
EasySep Mouse T cell Isolation Kit	StemCell Technologies	19851A
RNeasy Mini Kit	Qiagen	74104
Mouse α/β TCR RNA Kit	MiLaboratories	TMMR-001
Murine Tumor Dissociation Kit	Miltenyi Biotec	130-096-730
10X Genomics Single Cell Sequencing, GEX+TCR	10X Genomics	1000244; 1000252

Deposited data

Raw and processed genomic single cell RNA-seq data	Gene Expression Omnibus	[Database]: [GSE270954]
Processed deep TCR-seq data	Zenodo	[Database]: [https://doi.org/10.5281/zenodo.12550792]

Experimental models: Cell lines

MOC1	In house	RRID:CVCL_ZD32
------	----------	----------------

Experimental models: Organisms/strains

C57BL/6	Taconic	RRID:IMSR_TAC:B6
B6.SJL-Ptpr ^a Pepc ^b /BoyJ	Jackson Labs	RRID:IMSR_JAX:002014

Software and algorithms

ImageJ	National Institutes of Health	www.imagej.net/ij
FlowJo V10.8.1	FlowJo, LLC	Flowjo.com
Biorender	Biorender	www.biorender.com
Prism	GraphPad	https://www.graphpad.com/features
R	R Core Team, 2021	https://www.r-project.org/
CellRanger v7.0.1	10X Genomics	https://www.10xgenomics.com/support/software/cell-ranger/latest

RESOURCE AVAILABILITY

Lead contact

Further information and requests should be directed to Clint T. Allen; 240-858-7773; clint.allen@nih.gov.

Materials availability

This study did not generate unique reagents.

Data and code availability

- All individual mouse and human level data is included in the manuscript as individual data points and all raw data for each subfigure is included in the **Supplemental Data File**. All raw and processed genomic single cell RNA-seq data is publicly accessible through Gene Expression Omnibus ([Database]: [GSE270954]). Processed deep TCR-seq data is publicly accessible through Zenodo ([Database]: [<https://doi.org/10.5281/zenodo.12550792>]).
- This paper does not report original code.
- Any additional information required to reanalyze the data reported in this paper is available from the **lead contact** upon request.

EXPERIMENTAL MODEL AND STUDY PARTICIPANT DETAILS

Animals

All murine studies were performed after full review and approval by the NIH Animal Care and Use Committee. Wild type female C57BL/6 mice (B6NTac; RRID:IMSR_TAC:B6) aged 6-8 weeks were purchased from Taconic. Female CD45.1 transgenic mice (B6.SJL-*Ptprc^aPepc^b*/BoyJ; RRID:IMSR_JAX:002014) were purchased from Jackson Labs. Standard housing and husbandry conditions were used.

Human participants

Human PBMC specimens were acquired from a study that was approved by the institutional review board of the NIH, and each patient provided written informed consent. Clinical and demographic characteristics of these participants has been previously published.¹³

Cell lines

Original stocks of genomically characterized¹⁴ MOC1 cells (RRID:CVCL_ZD32) were a gift from Ravindra Uppaluri (Dana-Farber Cancer Institute, Boston, MA). Cells were maintained in the following culture media: IMDM/F12 (2:1) with 5% fetal calf serum, penicillin/streptomycin, 1% amphotericin, 5 ng/mL EGF (Millipore), 400 ng/mL hydrocortisone, and 5 μ g/mL insulin in standard incubator conditions.³⁶ Cells were used for experiments at low passage number (<30), maintained in sterile conditions and serially tested for murine associated pathogens and mycoplasma (Lonzo MycoAlert Mycoplasma Detection Kit).

METHOD DETAILS

Reagents

Therapeutic agents used in this study were obtained through a Cooperative Research and Development Agreement between EMD Serono and the NCI. Avelumab (α PDL1, MSB0010718C) was provided by the healthcare business of Merck KGaA, Darmstadt, Germany (CrossRef Funder ID: 10.13039/100009945) under a previous alliance between the healthcare business of Merck KGaA, Darmstadt, Germany and Pfizer. Bintrafusp alfa (α TGF- β + α PDL1, MSB0011359C, formerly known as M7824) and bintrafusp alfa with a mutated PDL1 binding domain (α TGF- β + α PDL1mut) were provided by EMD Serono (CrossRef Funder ID: 10.13039/100004755). All agents were diluted in sterile 1xPBS prior to use. Recombinant murine TGF- β was purchased from Biolegend (San Diego, CA).

Murine studies

Primary and secondary challenge tumors were established by subcutaneous injection of MOC1 tumor cells (5×10^6 cells/injection) in matrigel (30% by volume) purchased from R&D Systems (Minneapolis, MN). Tumor volume was measured at least twice weekly and was calculated as (length² x width)/2. For all treatment experiments, full (350 μ g) or reduced dose (35 μ g) avelumab, full (492 μ g) or reduced dose (49.2 μ g) bintrafusp alfa, bintrafusp alfa with a mutated (492 μ g) or sterile 1xPBS volume equivalent was administered on days 9, 11 and 13 via intraperitoneal (IP) injection. For all secondary tumor challenge experiments, challenge tumors were engrafted on day 15. Low endotoxin anti-mouse CD8a (clone RPM1-14) or CD4 (clone GK1.5) were purchased from BioXCell (Lebanon, NH). When used, CD8 and CD4 depleting antibodies were administered beginning one day before treatment (day 8), 200 μ g IP/injection, and continued twice weekly for three weeks. FTY-720 was purchased from Sigma. When used, FTY-720 was administered beginning two days before treatment (day 7), 30 μ g IP/injection, and continued every other day for three weeks.

Histologic analysis

Formalin-fixed paraffin-embedded tumors were sections and stained with hematoxylin and eosin as a commercial service by Histoserv (Germantown, MD). Pan cytokeratin immunohistochemistry was performed using the mouse anti-wide spectrum cytokeratin (Abcam) as previously described.³⁷ Images were acquired on a Vectra Polaris (Akoya Biosciences, Marlborough, MA).

T cell sorting from tumors and single-cell RNA- and TCR-sequencing

Tumor tissues from individual mice were processed into single-cell suspensions by mincing, chemical (Murine Tumor Dissociation Kit, Miltenyi, Gaithersburg, MD) and mechanical (gentleMACS Dissociator, Miltenyi) dissociation per manufacturer recommendations. Suspensions from five digested tumors per treatment condition were combined, filtered, washed with 1% BSA in PBS, nonspecific staining was blocked with anti-mouse CD16/32 (Biolegend) antibody, cells were stained with anti-mouse TCR- β (clone H57, Biolegend) and T cells were sorted to >99% purity on a BD FACS Aria III sorter. Cells were concentrated to 1000 cells/ μ l and loaded onto the Chromium Controller (10X Genomics, Pleasanton, CA) with a target of 10,000 cells per sample. Two captures per treatment condition were performed. Cells were mixed with barcoded gel beads and 5' GEM Kit v3 reagents and single cell capture was performed (10X Genomics). Following reverse transcription, cDNA and murine TCRs were amplified, and gene expression and TCR sequencing libraries were constructed according to the manufacturer's recommendations. Each DNA library was loaded into a sequencing lane on a NovaSeq system (Illumina, USA) and was sequenced with pair-end reads of 75 bp. Demultiplexing was done allowing 1 mismatch in the barcodes. UMI counts were obtained using Cell Ranger (v6.0.2).

T cell sorting from spleens and lymph nodes and deep TCR sequencing

Spleens and tumor draining lymph nodes from individual mice were mechanically dissociated, filtered, washed with 1% BSA in PBS, and T cells were isolated using the EasySep Mouse T cell Isolation Kit from StemCell Technologies (Vancouver, Canada). RNA was extracted from all sorted samples using the RNEasy Mini Kit from Qiagen (Hilden, Germany). Deep TCR sequencing was performed using the Mouse α/β TCR RNA Kit from MiLaboratories (Sunnyvale, CA) per manufacturer recommendations.

Bioinformatic analysis

The resulting demultiplexing was done allowing 1 mismatch in the barcodes. UMI counts and TCR sequences were obtained using Cell Ranger v2 (v2.0.1). TCR sequences were aggregated across technical replicates using cellranger aggr. The filtered feature matrices, output by cellranger, were analyzed using the programming language R (CITE) and the R package Seurat (CITE). Potential doublets were identified using the R package scds (CITE). As per the manufacturer's specifications, we assumed a doublet rate of 4.6%. For each cell `scds::cxds_bcnds_hybrid` was used to compute the doublet score; the 4.6% of cells with the highest doublet scores were removed from the analysis. In addition, we removed all cells with less than 250 or more than 5000 detectable genes, less than 500 unique molecular identifiers (UMIs) or more than 25% of mitochondrial or hemoglobin transcripts.

The UMI counts were normalized using `Seurat::NormalizeData`, variable features were identified using `Seurat::FindVariableFeatures` and the data was scaled using `Seurat::ScaleData(vars.to.regress = 'nCount_RNA')`. The principle components were obtained using `Seurat::RunPCA` with the variable features. To remove batch effects between treatment groups we used `harmony::RunHarmony(group.by.vars = 'treatment', reduction = 'pca')` available through the R package harmony (CITE). Uniform manifold approximation and projection (UMAP) were computed using `Seurat::RunUMAP(reduction = 'harmony')`; shared nearest neighbor graph was obtained using `Seurat::FindNeighbors(reduction = 'harmony')` and clusters were identified using `Seurat::FindClusters`.

Peripheral TCR-beta sequences were assigned to individual single-cells based on the CDR3 nucleotide sequences allowing no mismatches.

Flow cytometry

Tumor tissues were processed into single-cell suspensions as described above. Suspensions were filtered through a 70 μm filter and washed with 1% BSA in PBS prior to blocking nonspecific staining with anti-CD16/32 (Biolegend) antibody. Cell surface staining was performed using fluorophore-conjugated anti-mouse CD45 (clone 30-F11), C45.1 (A20), TCR- β (H57), CD4 (GK1.5), CD103 (2E7), CD25 (3C7) and CXCR3 (173) antibodies from Biolegend, and CD8 (53-6.7; BD Biosciences). The p15E:H-2Kb tetramer and associated anti-mouse CD8 antibody (KT15) were purchased from MBL International (Woburn, MA). Foxp3+ (MF-14, Biolegend) staining was performed with the Foxp3/Transcription Factor Staining Buffer Set (Thermo) as per the manufacturer protocol. pSMAD2^{S465/S467}/3^{S423/S425} (072-670, BD Biosciences) staining was performed after surface staining and by resorting to fixation with 4% PFA (USB corporation) and permeabilization with 90% MetOH (Sigma Aldrich). Archived frozen human PBMC were thawed, recovered, and used for flow cytometry as described.³⁸ Cells were stained with primary conjugated anti-human CD3 (OKT3; Biolegend), CD8 (SK1; BD Biosciences), CD4 (OKT4; Biolegend) and CXCR3 (G025H7; Biolegend) antibodies. Cell viability for all cells was assessed via staining with SytoxGreen (Thermo) or GhostDye Violet510 (Cytex Biosciences) dyes. All analyses were performed on a Fortessa cell analyzer (BD Biosciences, Franklin Lakes, NJ) running FACSDiva software and analyzed with FlowJo V.X10.0.7r2.

In vitro T cell studies

Spleens were mechanically dissociated, filtered, RBC depleted and washed with 1% BSA in PBS, and T cells were isolated using the EasySep Mouse T cell Isolation Kit from StemCell Technologies (Vancouver, Canada). T cells were cultured for 24h at a concentration of $10^6/\text{mL}$ in 24-well plates coated with $1\mu\text{g}/\text{ml}$ of purified anti-mouse TCR- β (H57; BD Biosciences) and $1\mu\text{g}/\text{ml}$ of purified anti-mouse CD28 (37.51; BD Biosciences) in RPMI-based media supplemented with fetal bovine serum. After 24 hours of activation, T cells were stimulated with recombinant mouse TGF- β 1 (Biolegend) at the indicated doses and for an additional 24-hour period, in the presence or absence of $1\mu\text{g}/\text{ml}$ of bintrafusp alfa or bintrafusp alfa with a mutated PDL1 binding domain. Cells were analyzed after stimulation by flow cytometry, data was captured on a Fortessa cell analyzer and analyzed with FlowJo.

In vivo cytotoxicity assay

Splenocytes were harvested from CD45.1 transgenic mice and labeled with either CellTrace Violet (CTV; Thermo) or CellTrace Yellow (CTY; Thermo) per manufacturer recommendations. CTV labelled splenocytes were pulsed with $10\mu\text{g}/\text{mL}$ of p15E₆₀₄₋₆₁₁ (KSPWF₆₀₄₋₆₁₁) for 1 hour. Cells were washed, mixed at a 1:1 ratio, and adoptively transferred into wild-type CD45.2 B6 MOC1 tumor-bearing mice. Four hours later, splenocytes were harvested, and flow cytometry was used to determine the ratio of CTV to CTY cells. Data was captured on a Fortessa cell analyzer and analyzed with FlowJo. Antigen-specific cell killing was determined as $1 - (r_{\text{injected}}/r_{\text{treated}}) \times 100$, where $r = (\% \text{CTY})/(\% \text{CTV})$.

Peripheral T cell tumor-specificity assay

CD8 T cells were isolated from spleens as described above. MOC1 cells were irradiated to 18Gy to be used as antigen presenting cells (APCs). Splenic CD8⁺ T cells and irradiated MOC1 APCs were co-cultured for 36 hours at 37°C at a 1:1 APC-to-TIL ratio. Negative controls

included co-culture of T cells or APC alone. T cells were exposed to eBioscience Cell Stimulation Cocktail (Thermo) as a positive control. Murine IFN γ ELISpot kits were purchased from R&D Systems and used per manufacturer recommendations. Spot counts were measured on an Immunospot ELISpot plate reader from Cellular Technology (Shaker Heights, OH).

QUANTIFICATION AND STATISTICAL ANALYSIS

Details of each experiment can be found in the Figure Legends. Significance between two sets of paired data was determined with a Wilcoxon test. Significance between survival curves was determined with a Log-rank test. Significance between multiple sets of linked data, such as tumor growth curves, was determined with analysis of variance (ANOVA) with repeated measure comparison. Significance between engraftment rates at individual timepoints was determined with a Fisher's exact test. Significance between two sets of unpaired data was determined with a Mann Whitney test. In all cases, significance was set at $P \leq 0.05$. All statistical analyses were performed using Graphpad Prism v10.0.3 or R.

ADDITIONAL RESOURCES

Clinical specimens used in this study were acquired under clinical trial NCT04247282.